

NASA Technical Paper 1268

LOAN COPY: RET
AFWL TECHNICAL
KIRTLAND AFB,



Application of Shock Tubes to Transonic Airfoil Testing at High Reynolds Numbers

William J. Cook, Michael J. Chaney,
Leroy L. Presley, and Gary T. Chapman

NOVEMBER 1978

NASA



NASA Technical Paper 1268

Application of Shock Tubes to Transonic Airfoil Testing at High Reynolds Numbers

William J. Cook and Michael J. Chaney
Iowa State University
Ames, Iowa

Leroy L. Presley and Gary T. Chapman
Ames Research Center
Moffett Field, California



National Aeronautics
and Space Administration

**Scientific and Technical
Information Office**

1978

TABLE OF CONTENTS

	<u>Page</u>
NOMENCLATURE	v
SUMMARY	1
INTRODUCTION	1
SHOCK-TUBE PERFORMANCE ANALYSIS FOR HIGH REYNOLDS NUMBER	
TRANSONIC TESTING	3
EXPERIMENTAL STUDY	5
Testing Time	6
Wall Boundary Layers	6
Influence of Walls on Flow Field	7
Airfoil Pressure Measurements	8
RESULTS	9
Schlieren Photography	9
Pressure Results	11
CONCLUDING REMARKS	16
APPENDIX A	17
APPENDIX B	25
REFERENCES	28



NOMENCLATURE

a	speed of sound
C_p	pressure coefficient, equation (5)
C_p^*	pressure coefficient at $M = 1$
c	airfoil chord length
M	Mach number
M_2	$\frac{u_2}{a_2}$
M_s	shock Mach number, $\frac{U_s}{a_1}$
m	molecular weight
OVS	oscilloscope vertical sensitivity, equation (6)
p	static pressure
Δp	pressure change indicated by pressure transducer
q	dynamic pressure, $\frac{\rho_2 u_2^2}{2}$
Re_c	chord Reynolds number, $\frac{u_2 c \rho_2}{\mu_2}$
Re_u	unit Reynolds number $\frac{Re}{x}$
R_u	universal gas constant
T	absolute temperature
TCF	transducer calibration factor, equation (6)
t	time
t_i	ideal region 2 test time
t'	time, $t' = 0$ when primary shock wave arrives at airfoil leading edge
U_s	primary shock wave velocity
u_2	test gas velocity behind primary shock wave measured in reference frame fixed to shock tube wall
x	distance
x_m	model distance from diaphragm, figure 1

Δy_r	vertical change in trace on pressure transducer record, equation (6)
γ	gas specific heat ratio
δ	velocity boundary-layer thickness
μ	viscosity coefficient
ρ	density
χ	mole fraction of argon

Subscripts:

c	based on airfoil chord length
ij	$()_i / ()_j$
1	test gas ahead of primary shock wave
2	test gas behind primary shock wave (see u_2 and M_2 also)
4	driver gas
∞	undisturbed flow remote from model (region 2 in present study)

APPLICATION OF SHOCK TUBES TO TRANSONIC AIRFOIL TESTING

AT HIGH REYNOLDS NUMBERS

William J. Cook* and Michael J. Chaney*

Iowa State University, Ames, Iowa

Leroy L. Presley and Gary T. Chapman

Ames Research Center

SUMMARY

The shock tube as a device to fulfill current needs for testing transonic airfoils at high Reynolds numbers is considered. Performance analysis of a gas-driven shock tube shows that transonic airfoil flows with chord Reynolds numbers of the order of 100×10^6 can be produced, with limitations being imposed by the structural integrity of the facility or the model. A study of flow development over a simple circular arc airfoil at zero angle of attack has been carried out in a shock tube at low and intermediate Reynolds numbers to assess the testing technique. Results obtained from schlieren photography and airfoil pressure measurements show that steady transonic flows similar to those produced for the same airfoil in a wind tunnel can be generated within the available testing time in a shock tube with properly contoured test section walls. The study indicates that the shock tube is an alternative facility for studying high Reynolds number transonic airfoil flows.

INTRODUCTION

Certain large present-day aircraft operate at flight conditions in which Mach numbers range up to unity and Reynolds numbers based on vehicle length are of the order of 1×10^9 (ref. 1). For advanced transonic aircraft, Reynolds numbers based on the airfoil mean aerodynamic chord length range to nearly 100×10^6 (ref. 2). These Reynolds numbers exceed the performance capabilities of existing wind tunnels by at least a factor of 5 for general aerodynamic testing. Hence, steps are presently being taken to correct the deficiency in high Reynolds number transonic testing capabilities.

Two facility concepts considered to satisfy the high Reynolds number transonic testing requirements are the Ludwieg tube tunnel (ref. 2) and the cryogenic wind tunnel (ref. 3). Either of these facilities as described in the references would be very large and extremely costly to build, but would permit testing of scale models of advanced aircraft and space vehicles.

Mechanical Engineering Department and Engineering Research Institute.

There is a need for a smaller, less costly high Reynolds number transonic testing facility, particularly one in which research and testing of two dimensional transonic airfoils can be carried out. One device that appears to fulfill these requirements is the shock tube. This report considers the various aspects of the use of a shock tube as a testing facility for studying the behavior of transonic airfoil flows at high Reynolds numbers.

The need for experimental studies of transonic flows arises from the fact that such flows over airfoils typically involve viscous effects, such as separation, that have a pronounced effect on the flow field. Transonic flows thus present very challenging problems to the analyst. Hence, results from experimental studies, particularly those at high Reynolds numbers, are desired for comparison with results of analytical studies.

Shock tubes have not been extensively used for airfoil testing; however, few instances of airfoil testing in the driven section of shock tubes have been reported. Geiger, Mautz, and Hollyer (ref. 4) were apparently the first to use a shock tube to investigate transonic and supersonic flows. Their investigation was carried out using a tube with a 5.1- by 17.8-cm cross section and was directed mainly toward a shadowgraph study of flow-field development over airfoils. Steady supersonic flows were obtained over an 8.1-cm chord double-wedge airfoil in 0.4-msec testing time, but transonic flows (Mach number 0.79) over another wedge-shaped airfoil with a 6.4-cm chord were observed to be marginally steady in the available testing time of 1.5 msec. Griffith (ref. 5) carried out a study of transonic flows over wedge profiles in a tube with a 10.2- by 45.7-cm cross section and a length of 11.6 m. The pressure distribution and flow pattern for two dimensional flow fields around wedges at Mach numbers between 0.85 and 1.80 were studied using a Mach-Zehnder interferometer at a chord Reynolds number of approximately 10^5 . The flow fields were observed to become steady. For subsonic Mach numbers, a steady pressure distribution over the wedge was achieved after about 0.35 msec.

Ruetenik and Whitmer (ref. 6) carried out a shock-tube study of subsonic flow over a 10 percent thick symmetric double-wedge airfoil to simulate gust-type flows. The shock tube used was 20 by 61 cm in cross section. Interferometric measurements yielding transient pressure distribution and aerodynamic coefficients indicated that steady flow around the airfoil was achieved. However, this study was limited to a Mach number of 0.4 and a Reynolds number of 0.65×10^6 .

In order to accommodate larger models, a 2.13-m diameter shock tube with a 15-cm diameter driver section was used by Varwig and Rosenman (ref. 7) for transonic and supersonic testing. However, the Reynolds and Mach numbers of the flows produced in this facility appear to be limited to the range available in wind tunnels.

The above-described studies seem to indicate that airfoil testing is feasible in shock tubes. However, investigations have been limited to low Reynolds number flows and have not adequately dealt with questions regarding the time required to establish steady flow, the quality of the steady flow, and the validity of data obtained in shock tubes at high subsonic speeds

relative to data obtained in conventional transonic wind tunnels. Hence, the present study was undertaken to investigate in detail the practicality of carrying out high Reynolds number transonic airfoil testing in shock tubes.

SHOCK-TUBE PERFORMANCE ANALYSIS FOR HIGH REYNOLDS NUMBER TRANSONIC TESTING

Figure 1 presents a schematic diagram of a conventional gas-driven shock tube with an airfoil model with chord length c mounted a distance x_m from the diaphragm. The upper part of the figure illustrates ideal shock-tube performance in the $t-x$ plane. Both the driver and driven sections are assumed to be long enough to eliminate reflected waves from entering region 2, the test region, at the model location.

The methods of reference 8 readily permit the ideal performance of a simple shock tube to be predicted. The quantities of immediate interest here are the Reynolds and Mach numbers relative to the model, the testing time, and the driver-to-driven gas pressure ratio, p_{41} . From similarity considerations, aerodynamic testing requires that the Mach and Reynolds numbers and the specific heat ratio γ in the test facility be the same as those that exist in flight. Thus, the test gas specific heat ratio should be that for air, but the test gas need not be air. Certain gases such as argon and carbon dioxide and argon and Freon 12 (dichloro-difluoro-methane) can be mixed to yield gas mixtures with $\gamma = 1.4$ that, because of larger mixture molecular weights, offer an advantage over air for high Reynolds number aerodynamic testing in shock tubes.

Considering the shock Mach number M_s to be the independent variable, the test Mach and Reynolds numbers and the ideal testing time can be written as,

$$M_2 = \frac{M_s (\rho_{21} - 1) / \rho_{21}}{(T_{21})^{1/2}} \quad (1)$$

$$\frac{Re}{cp_1} = \frac{M_s}{\mu_2} \left(\frac{\gamma_1 m_1}{R_u T_1} \right)^{1/2} (\rho_{21} - 1) \quad (2)$$

and

$$\frac{t_i}{x_m} = \frac{(m_1 / \gamma_1 R_u T_1)^{1/2}}{M_s (\rho_{21} - 1)} \quad (3)$$

In equation (1), the density and temperature ratios across the shock, ρ_{21} and T_{21} , are functions of M_s and γ_1 only since ideal gases with constant specific heats are considered. In equations (2) and (3), m_1 is the molecular weight of the test gas and in equation (2), c is a characteristic model length; that is, the airfoil chord length. The driver-to-driven gas pressure ratio may be written as

$$p_{41} = \frac{p_{21}}{\left\{ 1 - \frac{(p_{21} - 1)(\gamma_4 - 1)\alpha_{14}}{[4\gamma_1^2 + 2\gamma_1(\gamma_1 + 1)(p_{21} - 1)]^{1/2}} \right\}^\beta} \quad (4)$$

where $\beta = 2\gamma_4/(\gamma_4 - 1)$ and $\alpha_{14} = (T_1\gamma_1m_4/T_4\gamma_4m_1)^{1/2}$. Figure 2 presents the quantities in equations (1) through (4) in terms of M_g for three test gases of different molecular weight but with $\gamma_1 = 1.4$; air, argon-Freon 12 mixture ($\chi = 0.85$, $m_1 = 52.1$), and argon-carbon dioxide mixture ($\chi = 0.52$, $m_1 = 41.9$), where χ is the mole fraction of argon in the mixture that yields $\gamma_1 = 1.4$. Figure 2(a) shows M_2 as a function of M_g . This curve is the same for each of the test gases. The curves for p_{41} in figure 2(a) are for use of helium as the driver gas with $T_4 = T_1$, where T_1 is room temperature. For a given test gas, variation of M_g and hence M_2 can be obtained by varying p_{41} .

Although other driver modes can be considered, room-temperature helium as the driver gas is considered typical and will be employed for illustrative purposes. Figure 2(b) presents curves for the ideal testing time per unit model distance, t_i/x_m , equation (3), and the Reynolds number variable Re/cp_1 , equation (2). Figure 2(c) presents the dynamic pressure $q = \rho_2 u_2^2/2$ vs chord Reynolds number for a test Mach number of 0.850. The usual ideal gas relations were employed for the gases in the computations for figure 2. Constant specific heats were assumed for all gases considered. (Consideration of variable specific heats (see appendix A) for the carbon dioxide in the argon-carbon dioxide mixture will, however, change somewhat the mole fraction required to produce $\gamma_2 = 1.4$.) The viscosities of the gas mixtures were computed on the basis of the viscosities of the constituents using the method of Wilke (ref. 9).

A preliminary evaluation of shock-tube performance for high Reynolds number transonic testing can be made from the curves in figures 2(a) and 2(b). For the case of $M_2 = 0.85$ ($M_g = 1.82$), a chord length of 15 cm, a chord Reynolds number $Re_c = 100 \times 10^6$, and air as the test gas with room-temperature helium as the driver gas, the value required for p_1 is 16 atm and that for p_4 is 111 atm. These pressures present no insurmountable structural problems in shock-tube design. Thus, at least in theory, transonic shock-tube flows with very high Reynolds numbers can be generated.

For the argon-Freon 12 mixture as the test gas, the values required for p_1 and p_4 with $M_2 = 0.85$ and $Re_c = 100 \times 10^6$ are 12.8 and 72 atm, respectively. A similar reduction in p_1 and p_4 results from use of the argon-carbon dioxide mixture as the test gas. In view of the relatively high values required for both p_1 and p_4 in order to produce the desired high Reynolds number transonic flows, there is an obvious advantage in using the gas mixtures in place of air as the test gas.

As illustrated in figure 2(c), transonic testing at high Reynolds numbers would involve relatively high dynamic pressures that would produce

large model loads when lifting airfoils are tested. However, calculations indicate that model support devices can be designed to carry these loads.

With regard to testing time, figure 2(b) indicates that a possible advantage is present in terms of increased test time through use of the gas mixtures in place of air. From figure 2(b) at $M_2 = 0.85$, the values of t_i/x_m for the air, argon-carbon dioxide, and argon-Freon test gases are 1.14, 1.38, and 1.55 msec/m, respectively. The time required to establish steady flow over a given model in a shock tube depends primarily on model configuration and model length as well as on the Mach and Reynolds numbers. This time cannot easily be determined analytically. Previous experimental investigations have not dealt thoroughly with this subject. Hence, an important part of the present investigation deals with experimental study of the flow pattern development and determination of the time required to achieve steady transonic flows over an airfoil in the shock tube.

EXPERIMENTAL STUDY

An experimental study at Iowa State University of transonic flow over an airfoil at zero angle of attack was carried out in a gas-driven shock tube using air as the test gas. The study was conducted to determine if steady flow could be achieved within the available testing time and to determine if the resulting flows were of the quality necessary to permit useful transonic flow results to be obtained.

The shock tube used in this investigation has a driven section with a rectangular cross section of 15.2 by 7.6 cm and a length of 9.75 m. A large dump tank is attached to the downstream end of the driven section. The model station is located 8.53 m from the diaphragm. Mylar diaphragms ranging in thickness from 0.05 to 0.38 mm were used for most of the tests performed. Scribed aluminum diaphragms were used in a few of the tests to provide a check on the performance of the Mylar diaphragms. At a nominal Mach number of 0.85, flows with Reynolds numbers (based on the airfoil chord length) ranging up to about 2×10^6 can be generated in the shock tube when the present 2-cm-thick glass test section windows are used. This Reynolds number range, although limited, is nonetheless adequate for evaluating the testing concept.

The airfoil chosen for this study was a 12 percent thick biconvex circular arc airfoil with a chord of 7.6 cm. This airfoil profile was selected because of its simplicity and the availability of both experimental and analytical studies with which to compare results. The airfoil was mounted with zero angle of attack at the model station on the tube center line between windows by means of transverse pins extending into both the windows and the airfoil. This model arrangement resulted in a span-to-chord ratio (aspect ratio) of unity and placed the upper and lower walls 1 chord length above and below the airfoil.

Two methods were employed to study the development and the nature of the flow over the airfoil. One method involved use of Schlieren photography. (An airfoil model was mounted between 2-cm-thick glass windows.) The Schlieren

system, aligned to view the airfoil profile, provided photos of the flow development over the airfoil. The other method consisted of pressure measurement. A second airfoil model was instrumented with fast-response pressure transducers to measure both the pressure variation with time and the pressure distribution on the airfoil.

Testing Time

Prior to considering the flow development over the airfoil, the time available for testing will be discussed. Figure 3(a) shows for a range of subsonic Mach numbers the ideal testing time t_i at the model station determined from figure 2 with air as the test gas. In order to establish the actual testing time available, a constant-temperature, hot-wire anemometer was used to determine the time between shock-wave arrival at the model station and the arrival of the contact region between the driver and driven gases. The hot-wire system used was a Disa Model 55D05 anemometer with a 55A22 probe with a 1.2-mm-long, 5- μ wire. The wire was positioned perpendicular to the flow on the tube centerline without the airfoil in place.

A typical hot-wire response as recorded by an oscilloscope is shown in figure 3(b). The declining signal after shock-wave arrival is attributed to transient heating effects in the hot-wire support probe and is of no consequence since events in time are of most interest. Oscillations in the signal beginning at about 3.6 msec are interpreted as the arrival of the turbulent region in the flow formed as a result of the diaphragm bursting and marks the termination of the undisturbed region 2 flow (but not necessarily the arrival of the driver gas).

The testing times so determined from hot-wire responses are compared in figure 3(a) for both Mylar and aluminum diaphragms with testing times computed by applying the approximate rule that the actual testing time in a shock tube is one-half the ideal time. The experimental values are seen to fall below the curve for $t_i/2$ for the shock tube employed here. The experimentally determined turbulent-free times are near 40 percent of the ideal times. It is interesting to note that the use of Mylar diaphragms as opposed to aluminum diaphragms, which petal in a more ideal manner, does not influence the turbulent-free test time.

Wall Boundary Layers

In view of the relative sizes of the model and cross sectional area of the test section involved in aerodynamic testing in the present study, it is important to consider the boundary layers that form on the shock-tube walls in region 2, the test region. This boundary layer grows in an unsteady manner in a reference frame fixed to the model but may be considered steady in a coordinate system attached to the moving shock. At the high Reynolds numbers of interest here the boundary-layer flow is turbulent. The fraction of the airfoil span that is submerged in the sidewall boundary layer should be minimized.

Mirels (ref. 10) has treated the shock-tube sidewall turbulent boundary layer in detail. The boundary-layer thickness on the wall at the model station is shown as a function of time for the shock tube used for several values of Re_c ($c = 7.62$ cm) in figure 4(a) for $M_2 = 0.85$. The two smaller values of Re_c shown are in the Reynolds number range of the present study. The two larger values are included for illustrative purposes. The thickness curves in figure 4(a) assume that the boundary layer is turbulent immediately behind the shock and as a result tend to over-predict the thickness at early times and low Reynolds numbers. This is illustrated in figure 4(b) in which measurements of the boundary-layer thickness made from Schlieren photos of the turbulent sidewall boundary layer are compared with those predicted by the Mirels' method, and with Mirels' method corrected for the fact that the boundary layer remains laminar for a distance behind the shock. The method used to compute the corrected boundary-layer thickness involved assuming that the turbulent boundary layer grows from the approximate point at which boundary-layer transition takes place. This point, termed the virtual origin of turbulence, was established by assuming that transition took place at a Reynolds number of 7.5×10^5 based on conditions relative to the shock wave. The measured thicknesses and those predicted by application of Mirels' method using the virtual origin are in good agreement for the case shown. The results show that the correction for the virtual origin becomes less important with increasing time. Extrapolation of the results in figure 4(b) indicates that at 3 msec the virtual origin correction would be small and that the boundary-layer thickness is close to that predicted directly by Mirels' method.

It is seen from figure 4(a) that a sizable portion of the 7.60-cm span of the airfoil is submerged in the wall boundary layers by the end of the available testing time of approximately 3 msec (determined from fig. 3(a) at $M_2 = 0.85$). For $Re_c = 2 \times 10^6$, $2\delta/c = 0.46$; however, this figure can be somewhat misleading. The turbulent sidewall boundary-layer velocity profile can be approximated by the 1/7th power law. This indicates that the major portion of the velocity deficit is near the sidewall; for example, the fraction of the span covered to the point in the two sidewall boundary layers, where the velocity is 80 percent of the free-stream velocity, is 0.10. Accordingly, no large velocity gradients were expected in the spanwise direction for the major portion of the span.

Influence of Walls on Flow Field

A particularly important consideration in transonic testing facilities is the influence of the facility walls on the flow field around the model. One measure of this influence is the amount of blockage that results due to the presence of the model. This consideration is discussed extensively in reference 11. At a Mach number of 0.85, a blockage (cross-section area of the model to that of the flow channel) of about 2 percent causes choking. In order to avoid significant flow distortions, the actual blockage should be considerably less than 2 percent. It is evident in the present case that this condition is not satisfied.

Two methods are available to overcome blockage effects in aerodynamic test facilities. These are (1) use of perforated or slotted walls with adjacent chambers that tend to automatically regulate the flow around the model to render a flow pattern close to that encountered in free flight, and (2) use of walls contoured to match streamlines that occur in free flight. Although perforated and slotted walls have been used extensively in transonic wind tunnels, such walls have apparently not been used in aerodynamic testing in shock tubes.

In view of the complexities involved in design of a perforated or slotted test section, the method used to deal with blockage in the present study was wall contouring. The recent work of Murman and Cole (ref. 12) and Murman (ref. 13), which is based on transonic small disturbance theory, provides a means of obtaining potential flow stream surfaces as well as potential flow fields (including imbedded shock waves) for thin two-dimensional transonic airfoils at zero angle of attack. Due to their inviscid nature, such solutions would not be expected to accurately describe the flow field near the airfoil where boundary-layer effects are important, but would be expected to yield reasonably accurate results for the flow well away from the model.

The slope as a function of position for stream surfaces of the flow 1 chord length above and below the model was obtained by the methods of references 12 and 13¹ for the test airfoil at test Mach numbers of 0.83, 0.85, and 0.87. The influence of the time dependent turbulent side wall boundary layer was accounted for in an approximate manner in the computation of the final wall contour. This was done by computing the slope of the displacement thickness for the turbulent sidewall boundary layer by means of reference 10 and adding this slope algebraically to the slope of the stream surface. The resulting slope was then integrated with position to provide the final wall contours. The wall contours determined in this manner are shown in figure 5. Separate contours for the three Mach numbers were then machined into the blocks that compose the upper and lower walls of the test section. The contours extended from 1.8 chord lengths upstream of the leading edge of the airfoil to about 3 chord lengths downstream of the trailing edge.

Airfoil Pressure Measurements

As noted previously, one means of studying the airfoil flows generated was by means of pressure measurements made on the airfoil surface. Six small fast-response Kulite pressure transducers having rise times of approximately 10 μ sec were used.

The transducers were placed at midspan of the airfoil flush with the surface in 5-mm-wide spanwise grooves that also served as channels for the

¹The authors are indebted to Dr. Earll Murman for his consultation and for providing the computer program related to the methods of references 12 and 13.

transducer electrical leads. Paraffin wax used to cover the leads and fill the grooves was trimmed to maintain the airfoil profile. Figure 6 shows a photo of the instrumented airfoil, mounted on an aluminum disc which was machined to replace one of the glass windows. The transducer electrical leads were passed through rubber vacuum seals on the far side of the disc. The 15-cm scale provides a size reference. The numbers on the airfoil denote the six transducers, the sensing surfaces of which are located near the termination of the grooves. Transducers were placed at values of x/c of 0.20, 0.40, 0.60, 0.70, 0.80, and 0.88. This series of positions was designated as pattern A.

Due to the symmetry of the airfoil profile and wall contours, rotating the airfoil one-half turn to interchange the leading and trailing edges permitted measurements to be made at additional x/c locations of 0.12 and 0.30, and exchanged transducers at x/c positions at 0.20 and 0.80 as well as at 0.40 and 0.60. This series of positions was designated as pattern B. For some tests two gages were positioned at $x/c = 0.60$, one at midspan and one 2.5 cm away from midspan, in order to obtain an indication of any spanwise flow variation. Unless otherwise noted, the measurements discussed and presented herein are from tests in which the gages were located at midspan.

Figure 7 is a schematic of the pressure measurement system. The complete transducer circuit consists of an integrated circuit Wheatstone bridge formed on a silicon diaphragm and a temperature compensation module. The bridge was excited by means of a battery. The excitation voltage was monitored by a digital voltmeter. Use of dual beam oscilloscopes permitted two gage response records to be recorded on each Polaroid photo. A millivolt meter replaced the oscilloscope to calibrate the transducers. In order to obtain results that were as accurate as possible, the transducers were calibrated before each series of runs. This was accomplished by making static measurements of pressure and transducer voltage with the airfoil mounted in the test section of the shock tube. Several vacuum gages that are used to measure the test section pressure provided measurement and cross checks of the pressure in the desired range of calibration.

RESULTS

Schlieren Photography

Flow development over the airfoil was studied for each of the three wall contours by means of Schlieren photos taken at various times t' after arrival of the primary shock wave at the airfoil leading edge. Figure 8(a) shows a photo of the primary shock wave and the wave pattern generated at $t' \doteq 0.08$ msec. (The dark areas outside the airfoil profile at about 0.25 and 0.75 chord fractions are imperfections in the glass windows in the regions of the mounting pins and do not influence the flow over the airfoil.)

The circular wave in figure 8(a) continues to grow and in turn reflects from the upper and lower walls and the airfoil as the primary shock wave moves downstream. Figure 8(b) shows the wave pattern at $t' = 0.5$ msec. These waves disappear from the field of view as the shock wave moves further down the tube. At the nominal Mach number of 0.85, the photos obtained indicate that steady flow was established in 1.5 to 2.0 msec. Figures 8(c) and 8(d) present steady flow patterns observed. These photos are for $t' = 2.5$ msec and are typical of those obtained for values of t' ranging from 2 to 3 msec. The turbulent-free testing time from figure 3 at $M_2 = 0.85$ is about 3 msec. Thus, the Schlieren photos indicate that steady flow patterns were obtained within the available testing time.

Figures 8(c) and 8(d) illustrate the marked influence of Reynolds number on the steady flow patterns that were observed. For the flow in figure 8(c) with $Re_c = 0.27 \times 10^6$, the boundary layer is laminar over the forward half of the airfoil and at the entrance of the adverse pressure gradient region of the airfoil. This boundary layer first separates and then undergoes transition to form a large turbulent wake. A Mach line created by boundary-layer separation merges with the recompression shock to form a lambda wave configuration. The flow pattern in figure 8(c) exhibits all of the features of low Reynolds number flow over the same airfoil profile observed in a wind tunnel by Wood and Gooderum (ref. 14).

Figure 8(d) shows a photo of a flow at $Re_c = 2 \times 10^6$ in which boundary-layer transition occurred upstream of the adverse pressure gradient region. Here the shock-wave configuration is different from that in figure 8(c), as is the wake flow. This flow pattern is again similar to that observed by Wood and Gooderum in a wind tunnel for a turbulent airfoil boundary layer. The symmetry of the flows above and below the airfoil in the photos in figures 8(c) and 8(d) demonstrates that extremely uniform transonic flows are generated in the shock tube.

Shock-wave profiles like those in figure 8(d) permit comparison with the shock-wave profiles observed by Wood and Gooderum for turbulent airfoil boundary-layer flows. Such a comparison provides one means of evaluating the present experimental method. Figures 9(a), 9(b), and 9(c) present for the three wall contours a comparison of shock profiles measured from Schlieren photos taken at various M_2 values with those determined from interferograms by Wood and Gooderum. For the present results in figure 9, Re_c was 2×10^6 . Figure 9(d) presents a composite comparison of the results in figures 9(a), 9(b), and 9(c) that permits the influence of the wall contours to be assessed.

The results at $M_2 = 0.85$ and 0.87 shown for each contour indicate an influence of the wall contours on the shock profiles. The present results locate the shock waves downstream of those of Wood and Gooderum at corresponding Mach numbers. The results in figure 9(d) for walls contoured for flows at $M_2 = 0.87$ exhibit the best agreement with the results of reference 14 at both $M_2 = 0.87$ and 0.85.

Since the unit Reynolds number range was limited in the wind tunnel used by Wood and Gooderum, they used two methods to obtain turbulent flow over the

1-in. chord length airfoils tested. One method involved stretching a small-diameter wire across the test section about 1 chord length upstream of the airfoil leading edge to produce turbulence. The other involved extending a thin flat plate 1 chord length upstream along the airfoil chord line to generate a turbulent boundary layer over the airfoil. In the present study, the Reynolds number was large enough to permit natural boundary-layer transition to occur on the airfoil.

In view of the sensitivity of the shock-wave pattern to the nature of the airfoil boundary layer, it is likely that the differences in figure 9 between the present shock-wave profiles and those of reference 14 are attributable to the differences in the manner in which the turbulent boundary layer formed. This is borne out to some extent by Schlieren photos taken in the present study for flows at $Re_c = 1.25 \times 10^6$ over the airfoil with one flow surface smooth to permit natural boundary-layer transition and the other surface roughened to promote boundary-layer transition. Figure 10 shows one of these photos. (The dark area near the leading edge is a repaired fracture in one glass window.) It is seen that the shock profile for the roughened side lies upstream of the shock profile for the smooth side.

Pressure Results

Measurements of pressure at various locations on the airfoil surface were made using the model shown in figure 6 over the Mach number range $0.82 < M_2 < 0.88$ for each of the three wall contours with both laminar and turbulent airfoil boundary layers. Typical transducer response records for both the A and B gage patterns and for laminar airfoil boundary-layer flow (fig. 8(c)) are shown in figure 11(a). (The straight horizontal traces on the response records are reference traces for grid alignment.) The transducer records for all laminar boundary-layer runs exhibited the characteristics of those in figure 11(a). Regardless of the transducer location, however, the response records indicate that essentially steady pressure values were reached in 1.5 to 2 msec after flow initiation.

The transducer records for the gages located at values of $x/c \leq 0.70$ tend to exhibit less noise than do those further downstream where the records are characterized by high-frequency oscillations. From figure 8(c) it is seen that boundary-layer separation and transition occur at about $x/c = 0.6$ and that at x/c values near unity, a well-defined turbulent flow region exists.

The response records of runs for which the airfoil boundary layer was turbulent were similar to those for the laminar airfoil boundary-layer runs. Typical response records are shown for the turbulent case in figure 11(b) and are similar to those in figure 11(a).

In order to compare the present pressure results with those of other studies, pressure coefficients were computed from the response records of each transducer. In the pressure coefficient expression

$$C_p = \frac{p - p_\infty}{\frac{1}{2} \rho_\infty u_\infty^2} = \frac{(p/p_\infty) - 1}{\gamma M_\infty^2 / 2} \quad (5)$$

the quantities with subscript ∞ were taken as those computed behind the incident shock (region 2, fig. 1), since that flow is assumed to be the incoming flow to the airfoil. Measurement of the shock speed upstream of the airfoil test section and the temperature T_1 permitted the shock Mach number M_s to be calculated. Assuming the usual normal shock relations for air and taking $\gamma_{\text{air}} = 1.4 = \text{constant}$, T_{21} , p_{21} , and ρ_{21} can readily be computed, as can the value of M_2 by use of equation (1). Then,

$$p_\infty = p_2 = p_{21} p_1$$

and

$$p = p_1 + \Delta p$$

where p is the local airfoil pressure and Δp is the pressure change (as indicated by the pressure transducer) from the measured pressure p_1 . The expression for Δp is

$$\Delta p = (\Delta y_r, \text{cm})(OVS, \text{mV/cm})(TCF, \text{torr/mV}) \quad (6)$$

where Δy_r is the vertical change on the oscilloscope record measured from the trace just prior to the step at shock arrival to the steady state segment of the trace, usually taken at 2 to 2.5 msec. The terms *OVS* and *TCF* are, respectively, the oscilloscope vertical sensitivity and the transducer calibration factor.

The pressure coefficient results shown in terms of Mach number M_2 in figures 12(a) and 12(b) are for laminar airfoil boundary-layer flows and the 0.83 Mach number wall contour. These results are typical of those obtained for the laminar flow case in this study and are associated with the flow pattern shown in figure 8(c). Shown for comparison purposes in figure 12(a) are the pressure coefficient curves obtained from the experimental results of Wood and Gooderum (ref. 14) for laminar boundary-layer flow over the same airfoil profile tested here. Also shown are theoretically predicted results for the pressure coefficient C_p vs x/c obtained by the methods of references 12 and 13 for the same airfoil.

As noted previously, transducer patterns A and B have common values of x/c of 0.20, 0.40, 0.60, and 0.80. Therefore, results from two transducers were obtained at these locations. The curves marked A and B in figure 12(a) are straight lines fitted to the data points for the transducer patterns A and B. At values of $x/c = 0.4$ and below, the data exhibited essentially straight line behavior. At larger values of x/c , after boundary-layer separation, figure 12(b), the results do not follow this pattern as clearly.

The data in figure 12(a) exhibit some scatter about the fitted lines. An approximate error analysis was performed for a typical point in a typical run in order to assess the uncertainty in C_p . The details are given in appendix B. Random errors in all of the measured quantities were assessed. The data point chosen as typical was the point at $M_2 = 0.844$ and $x/c = 0.4$ for transducer pattern A in figure 12(a). The analysis produced $C_p = -0.45 \pm 0.04$. The band of uncertainty in C_p is shown in figure 12(a) about the chosen point. The result seems consistent with the scatter of the data in that the scatter seems to be within the error band.

By fitting a curve through the collection of data points for a given gage pattern, as with curves A and B in figure 12(a), or by examining the collective results in figure 12(b), more representative results at a given Mach number can be obtained. Values of C_p vs x/c determined from figures 12(a) and 12(b) at $M_2 = 0.83$ in this manner are shown in figure 12(c). Results for wall contours for $M = 0.85$ and 0.87 with a laminar airfoil boundary layer obtained at the corresponding Mach numbers are shown in figures 12(d) and 12(e), respectively. These results were obtained by the same method used for figure 12(c).

Also shown in figures 12(c), 12(d), and 12(e) is the pressure coefficient C_p^* which is the C_p value at $M = 1$. In order to check the influence of diaphragm performance on results, aluminum diaphragms were used in place of Mylar diaphragms in some of the $M = 0.87$ contour tests. These results are shown in figure 12(e) and are not significantly different from the results obtained using Mylar diaphragms.

At this point it is appropriate to comment further on the pressure coefficient results of reference 14, which are shown in figures 12(c), 12(d), 12(e), and 12(f). These were obtained for low Reynolds number wind-tunnel flows over a 1-in. chord length airfoil from reduction of data from interferograms. Evaluation of pressure distribution by interferometric means is limited to the laminar boundary-layer regime. The method is less accurate after boundary-layer separation and is not applicable to the turbulent regime. As a result, the laminar measurements of Wood and Gooderum terminate just beyond mid-chord.

Included for comparison purposes in figures 12(c), 12(d), 12(e), and 12(f) is the C_p variation with x/c predicted by the method of references 12 and 13 at the Mach number of the corresponding flow. Due to the inviscid limitation of this method, it would not be expected to yield correct C_p values after boundary-layer separation or in other regions wherein viscous effects are dominant. The results of Wood and Gooderum and those obtained by Murman's method are in good agreement over the forward half of the airfoil.

The present results for each contour exhibit generally good agreement with those of reference 14 for the forward half of the airfoil where the results of reference 14 are expected to be the most accurate. Further downstream, where the results of reference 14 are probably less reliable, the present results differ somewhat from those of reference 14 and indicate the

expected pressure increase near the trailing edge. The generally good agreement of the present results with the results of reference 14 provides further evidence that transonic flows like those observed in wind tunnels can be produced in shock tubes.

Figure 12(f) shows the present low Reynolds number results in terms of the pressure coefficient C_p vs x/c obtained at a flow Mach number of 0.85 for each of the three wall contours. A small influence of the wall contours is evident for the results in figure 12(f) from inspection of the results for the wall contours designed for $M = 0.83$ and 0.87 flows. The largest effect occurs near the trailing edge. Results for the pressure coefficient at $M = 0.85$ obtained in the present studies at low Reynolds numbers with no wall contouring (i.e., with straight walls) are also shown in figure 12(f). These results deviate significantly from the other results and clearly indicate the necessity for considering wall effects.

Figure 13 presents results for the case of a turbulent airfoil boundary layer in the same format used for the laminar case in figure 12. Figures 13(a) and 13(b) show pressure coefficient results in terms of M_2 for each x/c location for the 0.83 Mach number wall contour. These results are typical of those for the other wall contours for the turbulent case. Generally, the results for a fixed gage location for a given gage pattern exhibit less scatter about the straight lines in figures 13(a) and 13(b) than do those for the laminar case in figures 12(a) and 12(b). The results for the two transducer patterns at both $x/c = 0.4$ and 0.6 depart from each other by amounts that rule out attributing the differences to random errors. These differences will be discussed later.

The slopes of the curves fitted to the results in figures 13(a) and 13(b) differ somewhat from those of Wood and Gooderum (laminar flow) and from those predicted by Murman's inviscid computation method. This is attributed mainly to the fact that the wall contour is designed only for a flow Mach number of 0.83. Up to boundary-layer separation, pressure coefficient results for the inviscid, laminar, and turbulent cases should not differ significantly.

Figure 13(c) presents results in terms of C_p vs x/c for the turbulent case obtained at $M_2 = 0.83$ from figures 13(a) and 13(b) ($M = 0.83$ wall contour). Also shown for comparison purposes are the laminar results of Wood and Gooderum and the C_p variation predicted by Murman's method, with the latter shown up to the apparent separation point. Figures 13(d) and 13(e) present similar results for Mach numbers 0.85 and 0.87 which were determined using corresponding wall contours.

The results given in figures 13(c), 13(d), and 13(e) show further that the measurements for the A and B transducer patterns at fixed locations did not agree in all cases; a possible explanation lies in the location of the transducers within the two patterns. Referring to figure 6, it is noted that the transducers for the A pattern are clustered rearward and for the B pattern they are clustered forward. Since small but unavoidable surface roughness was present as a result of the manner in which the transducers were installed on the airfoil, it is possible that the difference in the roughness position that

occurs in switching from the A to B patterns caused boundary-layer transition to occur differently, that is, further forward for the B pattern, and thus produced the noted differences in C_p .

Some tests were run for the turbulent boundary-layer case with the gage pattern for which two gages were positioned at $x/c = 0.60$, one at midspan and the other 2.5 cm away from the midspan location. The pressure coefficient results obtained from these two gages in several tests were found to be within about 8 percent of each other with neither gage indicating results consistently different from the other. This indicated that there was no significant spanwise variation in the flow.

Figure 13(f) presents the present results for the turbulent boundary-layer case in terms of C_p vs x/c for a Mach number of 0.85 obtained for each of the three wall contours. The results in figure 13(f) are similar for each wall contour except for the apparent orderly dependence on wall contour at $x/c = 0.80$ and 0.88. At the $x/c = 0.7$ location, the dashed line between the two points for the 0.87 contour is shown to indicate that an unsteady periodic-like pressure variation with time was observed. (Otherwise, as previously noted, all results are based on the time-steady segment of the transducer response curve.) The two end points represent the limits of the pressure variation. From figure 9(d) it is seen that the shock-wave profile for $M_2 = 0.85$ and the 0.87 contour, when extrapolated to the airfoil surface, intersects it at about $x/c = 0.70$. This suggests that the observed pressure fluctuations are due to an unsteadiness in the shock position near the airfoil surface. A similar behavior was observed for the $M = 0.85$ contour in the vicinity of $M_2 = 0.83$.

The results in figure 13, when compared to the corresponding results in figure 12, show agreement with the well-established fact that turbulent airfoil boundary layers separate farther downstream on the airfoil than do laminar boundary layers. Further, the pressure distributions follow the expected pattern in that for the turbulent case, the pressure decreases to lower values on the airfoil and exhibits higher values near the trailing edge when compared to the pressures for the laminar case.

Local Mach numbers on the airfoil up to the separation point can be estimated by using the measured pressure distribution and assuming that the flow from upstream is isentropic. Figures 14(a), 14(b), and 14(c) show the local Mach numbers vs x/c computed in this manner from the pressure distributions for the turbulent airfoil boundary-layer cases in figures 13(c), 13(d), and 13(e) at Mach numbers of 0.830, 0.850, and 0.870, respectively. Due to the isentropic limitation, the computations were terminated at the apparent separation point. Also shown for comparison purposes in figure 14 are curves for local Mach number vs x/c determined by Wood and Gooderum from their interferometer measurements for laminar airfoil boundary layers. As noted previously, the measurements of Wood and Gooderum were limited to the laminar case. The agreement with the present results is good for the forward half of the airfoil. As expected, the figures indicate that higher local Mach numbers are reached for the turbulent airfoil boundary-layer case.

CONCLUDING REMARKS

Results of this study demonstrate that two-dimensional transonic airfoil flows similar to those observed in wind tunnels can be generated in shock tubes when test section wall contouring is employed. Schlieren photos and other measurements show that the flows produced in the test section are very uniform and free of turbulence. Thus, airfoil testing can be accomplished in flows that are relatively disturbance-free when compared to some wind-tunnel flows. Analysis of shock-tube performance predicts that transonic airfoil flows with very high chord Reynolds numbers can be generated. Although the present study was limited to a maximum chord Reynolds number of 2×10^6 , there appears to be no reason why very high Reynolds number flows could not be generated in practice. The large shock tube described in reference 15 and located at the NASA Ames Research Center is suitable for producing such flows.

Although the results obtained are somewhat sensitive to wall contour, the requirement for wall contouring in shock-tube-airfoil testing is not viewed as a serious limitation. This is especially true where results from such tests are to be used to check analytical techniques that can accommodate effects of the wall.

Ames Research Center

National Aeronautics and Space Administration

Moffett Field, Calif., 94035, April 19, 1978

APPENDIX A

SHOCK-TUBE PERFORMANCE CONSIDERING VARIABLE SPECIFIC HEATS

The shock tube performance curves in figure 2 assume ideal gas behavior and constant specific heats. These assumptions are valid for the case of air as the test gas, but may not be acceptable for the mixtures considered. The influence of the assumptions for the argon-carbon dioxide mixture has been considered and is discussed below. Before testing is carried out using the argon Freon-12 mixture the above assumptions should be further evaluated.

The assumption of the ideal gas equation of state $p = \rho R_u / (m) T$ is considered adequate for the constituents of the argon-carbon dioxide mixture. In addition, the specific heats of argon are constant over a wide range of temperature. However, the specific heats of carbon dioxide exhibit relatively pronounced variations with temperature. It is considered important to maintain the specific heat ratio γ_2 equal to 1.40. Thus, it is necessary to determine for the case of variable specific heats the mole fraction of argon and the value of M_g that will produce the desired M_2 with $\gamma_2 \equiv 1.40$. A computer program was written to carry out the necessary computations. The flow chart for the program is shown in figure 15. A complete listing of the program is presented in table 1.

Figure 16 presents a comparison of some of the results obtained using the computer program with corresponding results obtained by assuming constant specific heats. The curve χ vs M_g (long dashes) was obtained using the computer program and imposing the condition $\gamma_2 \equiv 1.40$. (In this case $\gamma_1 \neq 1.40$.) Also shown is the value $\chi = 0.52$ obtained from the constant specific heat solution, that is, $\gamma_2 = \gamma_1$ (short dashes). Noting that with variable specific heats, χ is only a weak function of M_g , χ was fixed at 0.64 (i.e., the γ and Mach number decisions were bypassed in fig. 15) and the results presented as solid curves were obtained.

The results for M_2 vs M_g are essentially the same for both constant specific heats ($\chi = 0.52$) and variable specific heats ($\chi = 0.64$) so only one curve is shown. The quantity $\gamma_2 - 1$ is for all practical purposes equal to 0.40 when χ is taken as 0.64. For constant specific heats the sonic velocity $a = 16.66 T^{1/2}$, m/sec, and for variable specific heats $a = 17.08 T^{1/2}$ m/sec, where T is in degrees Kelvin.

Although the differences between the variable and constant specific heat results and curves are not large, the influence of the difference on the flow variables is not necessarily negligible. This is best illustrated by a numerical example. Consider a shock-tube test planned and carried out first on the basis of the constant specific heat solution and second on the basis of the variable specific heats solution. Let the desired test Mach number M_2 be 0.877 for each case and let $T_1 = 297$ K. Table 2 presents a comparison of the results obtained for both cases. Inspection of the results, particularly

those for U_g , indicates that significant errors would be introduced by assuming constant specific heats for carbon dioxide in the argon-carbon dioxide mixture.

C NORMAL SHOCK SOLUTION FOR IDEAL GAS WITH VARIABLE SPECIFIC HEAT.
 C MAIN PROGRAM IS SIMULTANEOUS SOLUTION OF FANNO, RAYLEIGH, AND
 C STATE EQUATIONS, WITH VARIABLE SPECIFIC HEAT, ACROSS A NORMAL
 C SHOCK. ONE EQUATION IN T2 RESULTS FROM ELIMINATING OTHER
 C VARIABLES IN THE EQUATIONS. ITERATION IS USED TO FIND T2 TO
 C SATISFY THE TEMPERATURE EQUATION. KNOWING T2, OTHER PROPERTIES
 C BEHIND THE SHOCK CAN BE FOUND.
 C
 C THE SPECIFIC HEAT, CP, OF ONE GAS (CO2) IS VARIABLE (SEE SUB
 C ROUTINE) IN THIS PROGRAM. THE OTHER GAS (ARGON) HAS CONSTANT CP
 C OVER A LARGE TEMPERATURE RANGE.
 C A SUBROUTINE IS PROVIDED TO CALCULATE THE VISCOSITY OF THE
 C MIXTURE AT T2.
 C
 C GIVEN T1, P1, SMN, AN INITIAL X, CPA, WA, AND WCO2, THE MAIN
 C PROGRAM WILL ITERATE ON T2 TO SOLVE TEMPERATURE EQUATION. THEN
 C G2 IS CALCULATED AND COMPARED TO GS--IF NOT WITHIN A SPECIFIED
 C TOLERANCE THE PROGRAM WILL ADJUST X, REPEAT THE T2 ITERATION
 C AND COMPUTE A NEW G2. IF ITERATION ON G2 IS NOT DESIRED INSERT
 C BLANK FIRST CARD IN DATA DECK. FOR G2 ITERATION, INSERT THE
 C FIRST CARD WITH A POSITIVE NUMBER.
 C
 C ITERATION ON TMN TO A SPECIFIED VALUE IS PROVIDED BY ADJUSTING SMN
 C FOR ITERATION, PLACE POSITIVE NUMBER ON THE SECOND DATA CARD.
 C FOR NO ITERATION ON TMN, LEAVE SECOND DATA CARD BLANK.
 C
 C ***** EXPLANATION OF SYMBOLS *****
 C (STATE 1 AHEAD OF SHOCK, STATE 2 BEHIND SHOCK)
 C T1, T2 = TEMPERATURE, (DEGREES RANKINE)
 C P1, P2 = PRESSURE, (LBF/SQ FT)
 C V1, V2 = SPECIFIC VOLUME, (CU. FT/ LBM)
 C POH21 = DENSITY RATIO OF STATE 2 TO 1
 C X = MOLE FRACTION OF ARGON
 C CPA = SPEC. HEAT AT CONSTANT PRES. FOR ARGON, (B/LBMOL-R)

TABLE 1.- Continued

```

C      CPC1,CPC2 = SPEC. HEAT AT CONS. PRES. FOR CO2, (B/LBMOL-R)
C      CPM1,CPM2 = SPEC. HEAT AT CONS. PRES. FOR MIXTURE, (B/LBMOL-R)
C      CVM1,CVM2 = SPEC. HEAT AT CONS. VOL. FOR MIXTURE, (B/LMBOL-R)
C      G1, G2 = RATIO OF SPEC. HEATS FOR MIXTURE
C      GS = IDEALLY DESIRED GAMMA 2 (G2)
C      G4 = RATIO OF SPEC. HEATS FOR DRIVER GAS
C      WM = MOLECULAR WEIGHT OF MIXTURE
C      WA = MOLECULAR WEIGHT OF ARGON
C      WCO2 = MOLECULAR WEIGHT OF CO2
C      WD=MOLECULAR WEIGHT OF DRIVERGAS
C      PM = MIXTURE GAS CONSTANT
C      SMN = SHOCK MACH NUMBER
C      TMN=TEST MACH NUMBER, (IN REGION 2)
C      A1, A2 = SPEED OF SOUND, (FT/SEC)
C      AT = A1/(SQRT(T1)) = SPEED OF SOUND PARAMETER.
C      U1 = VELOCITY OF PRIMARY SHOCK, (FT/SEC)
C      U2 = VELOCITY IN REGION 2, (FT/SEC) (RELATIVE TO WALL)
C      U2S = U2 IN SHOCK FIXED COORDINATES
C      FA = MASS FLOW PER UNIT AREA, (LBM/SQ. FT)
C      AVISM = VISCOSITY OF MIXTURE AT T2, (LBM/FT-SEC)
C      UNRE = UNIT REYNOLDS NUMBER = RE/X*P1, (L/M-ATM)
C      UNREP = UNIT REYNOLDS NUMBER, (1/MM-TORR)
C      B,C,D,E = CONSTANTS INVOLVED IN SIMULTANEOUS SOLUTION

C      *** MAIN PROGRAM ***
C
1      P1=100.0
2      SMN=1.735
3      X=0.64
4      CPA=4.960
5      GS=1.4000
6      WA=39.9
7      WCO2=44.0
C      EPSILON = EPSIL = CONVERENCE TOLERANCE FOR G2
8      EPSIL=0.001

```

TABLE 1.- Continued

```

C      DELTA = CONVERGENCE TOLERANCE FOR TMN
9      DELTA = 0.002
10     NR=5
11     NP=6
12     READ(NR,100) SET
13     IF (SET) 2,2,3
14     2 WRITE(NP,22) SET
15     22 FORMAT(3X,'SET=',F5.2,2X,'NO ITERATION ON G2')
16     GO TO 9
17     3 WRITE(NP,23) SET
18     23 FORMAT(3X,'SET=',F5.2,2X,'ITERATION ON G2')
19     9 READ(NR,100) TOP
20     IF (TOP) 4,4,5
21     4 WRITE(NP,24) TOP
22     24 FORMAT(3X,'TOP=',F5.2,2X,'NO ITERATION ON TMN')
23     GO TO 10
24     5 WRITE(NP,25) TOP
25     25 FORMAT(3X,'TOP=',F5.2,2X,'ITERATION ON TMN')
26     10 READ(NR,96) T1
27     WRITE(NP,98) T1
28     READ(NR,105) G4, WD
29     WRITE(NP,102) G4, WD
30     98 FORMAT(3X,'T1-',F7.1)
31     96 FORMAT(F7.1)
32     TT=0.80
33     GO TO 13
34     12 TT=TT+0.05
35     13 CONTINUE
36     GO TO 8
37     40 SMN=SMN+0.005
38     GO TO 8
39     41 SMN=SMN-0.005
40     GO TO 8
41     6 X=X-0.005
42     GO TO 8
43     7 X=X+0.005

```

TABLE 1.- Continued

```

44      8 WRITE(NP,106) X
45      WRITE(NP,107) SMN
46      XCPA=X*CPA
47      CPC1=CP(T1)
48      CPM1=XCPA+(1-X)*CPC1
49      CVM1=CPM1-1.986
50      G1=CPM1/CVM1
51      WM=X*WA+(1-X)*WC02
52      RM=1545.0/WM
53      A1=SQRT(G1*RM*32.2*T1)
54      U1=SMN*A1
55      V1=(RM*T1)/P1
56      1 FA=U1/V12      3      4      5      6      7
57      C=P1+(V1/32.2)*FA*FA
58      D=((4.0*RM)/32.2)*FA**2
59      E=(WM/50103.0)*FA**2*RM**2
60      B=XCPA*T1+(1-X)*(16.2*T1-6530.0*ALOG(T1)-(1.41E+6)/T1)+FA**2
61      1*V1**2*WM/50103.0
62      T2=T1*((1.0+(G1-1.0)*SMN**2/2.0)*((2.0*G1*SMN**2/(G1-1.0))-1.0))
63      1/((G1+1.0)**2*SMN**2/(2.0*(G1-1.0)))
64      GO TO 17
65      15 T2=T2+1.0
66      GO TO 17
67      16 T2=T2-1.0
68      17 Y=-B+(E*T2*T2)/((0.5*(C+SQRT(C*C-D*T2)))**2)+XCPA*T2+(1-X)
69      1*(16.2*T2-6530.0*ALCG(T2)-(1.41E+6)/T2)
70      IF ((Y) .LT. 7.0 .AND. (Y) .GT. -7.0) GO TO 18
71      IF (Y) 15, 18, 16
72      18 CPC2=CP(T2)
73      CPM2=XCPA+(1-X)*CPC2
74      CVM2=CPM2-1.986
75      G2=CPM2/CVM2
76      C IF SET .GT. 0.01 PROGRAM WILL ITERATE ON G2.
77      C IF SET .LT. 0.01 PROGRAM WILL NOT ITERATE ON G2, AND VALUE OF
78      C X WILL NOT BE CHANGED FROM INPUT VALUE.

```

TABLE 1.- Continued

```

73      IF (SET) 20, 20, 19
74      19 IF ((G2-GS)) 30, 20, 30
75      30 IF (ABS(G2-GS) .LT. EPSIL) GO TO 20
76      IF (G2-GS) 7, 20, 6
77      20 CONTINUE
78      P2=0.5*(C+SQFT(C**2-D*T2))
79      P21=P2/P1
80      T21=T2/T1
81      V2=RM*T2/P2
82      ROH21=V1/V2
83      U2S=FA*V2
84      U2=U1-U2S
85      A2=SQRT(G2*RM*32.2*T2)
86      TMN=U2/A2
87      AVISM=1.0*VISM(T2,X,WA,WC02)
88      UNRE=(SMN*A1*(ROH21-1.0)*6944.88)/(AVISM*RM*T1)
89      UNREP=UNRE/7.6E+5
90      ZINV=(2.*G4)/(G4-1.)
91      A4=SQRT(G4*32.2*1544.*T1/WD)
92      P41=P21/((1.-((G4-1.)/2.)*U2/A4)**ZINV)
93      AT=A1/(SQRT(T1))
94      WRITE(NP,101) X, G1, G2, P21, T21, RCH21, TMN
95      WRITE(NP,104) AT, P41
96      WRITE(NP,103) UNRE, UNREP
97      100 FORMAT(5F12.3)
98      101 FORMAT(3X,'X=',F8.5,3X,'G1=',F8.5,3X,'G2=',F8.5,3X,'P21=',F8.5,
99          13X,'T21=',F8.5,/,3X,'FCH21=',F8.5,3X,'TMN=',F8.5)
100     102 FORMAT(3X,'G4=',F6.2,3X,'WD=',F6.2)
101     103 FORMAT(3X,'UNRE=',E12.5,3X,'UNREP=',E12.5)
102     104 FORMAT(3X,'AT=',F8.4,3X,'P41=',P6.2)
103     105 FORMAT(3X,2F6.2)
104     106 FORMAT('0',4X,'X=',F6.3)
107     107 FORMAT(3X,'SMN=',F6.3)
C      IF TOP .GT. 0.01 PROGRAM WILL ITERATE ON TMN.
C      IF TOP .LT. 0.01 PROGRAM WILL NOT ITERATE ON TMN, AND VALUE OF
C      SMN WILL NOT BE CHANGED FROM INPUT VALUE.

```

TABLE 1.- Concluded

```

105      IF (TOP) 97, 97, 95
106      95 CONTINUE2      3      4      5      6      7
107      IF (ABS(TMN-TT) .LT. DELTA) GO TO 97
108      IF (TMN-TT) 40,97,41
109      97 CONTINUE
110      IF (TT .LT. 0.86) GO TO 12
111      99 STOP
112      END
C      SUBPROGRAM FOR SPECIFIC HEAT OF CO2 (JONES AND HAWKINS)

113      FUNCTION CP(T)
114      AA=16.2
115      BB=6530.0/T
116      CC=1.41E+6/T**2
117      CP=AA-BB+CC
118      RETURN
119      END
C      SUBPROGRAM FOR VISCOSITY OF GAS MIXTURE

120      FUNCTION VISM(T,X,WA,WCO2)
121      VISA=(1.451E-7)*T**0.739
122      VISC=((7.792E-7)*T**1.50)/(T+420.0)
123      VIS1=VISA/VISC
124      DM1=WA/WCO2
125      R1=(0.35355/(SQRT(1.0+DM1)))*(1.0+SQRT(VIS1)*(1.0/DM1)**0.25)**2
126      S1=X+(1.0-X)*R1
127      DM2=WCO2/WA
128      VIS2=VISC/VISA
129      R2=(0.35355/(SQRT(1.0+DM2)))*(1.0+SQRT(VIS2)*(1.0/DM2)**0.25)**2
130      S2=X*R2+(1.0-X)
131      VISM=(X*VISA)/S1+((1-X)*VISC)/S2
132      RETURN
133      END

```

TABLE 2.- COMPARISON OF RESULTS FOR THE CASE $M_2 = 0.877$ and $T_1 = 297$ K

Argon-Carbon Dioxide Test Gas Mixture

	a_1 , m/sec	M_s	U_s , m/sec	p_{21}	Re/cp_1 , (m atm) ⁻¹	p_1^a , atm	p_4^a , atm
Constant specific heat solution, $\gamma_1 = 1.4$ $\chi = 0.52$	287.1	1.853	532.0	3.840	0.490×10^8	13.43	91.17
Variable specific heat solution, $\gamma_2 = 1.40$ $\chi = 0.64$	294.4	1.853	545.5	3.938	0.472×10^8	13.90	95.64

^a Values of pressure required to produce $Re_c = 100 \times 10^6$ with $c = 15.24$ cm.

APPENDIX B

UNCERTAINTY IN PRESSURE COEFFICIENT RESULTS

The method used to estimate the uncertainty in the pressure coefficient results obtained by equation (5) is described by Kline and McClintock (ref. 16). When the result R for a single-sample experiment is known to depend on n independent variables v , the uncertainty interval w_R in the result is related to the uncertainty interval of each of the variables by:

$$w_R = \left[\left(\frac{\partial R}{\partial v_1} w_1 \right)^2 + \left(\frac{\partial R}{\partial v_2} w_2 \right)^2 + \dots + \left(\frac{\partial R}{\partial v_n} w_n \right)^2 \right]^{1/2} \quad (B1)$$

In most cases it is necessary to estimate the uncertainty interval for each variable (to specified odds) since such information is not usually statistically known. Table 3 presents the list of variables that enter into the computation of C_p , nominal values of the variables, and the values of the corresponding terms in equation (B1). The values of w_i were estimated based on 10 to 1 odds, and the values $\partial C_p / \partial v_i$ were obtained numerically by use of the computer program used to compute C_p values.

TABLE 3.- UNCERTAINTY ANALYSIS FOR A TYPICAL RUN; LAMINAR

AIRFOIL BOUNDARY LAYER. $M_2 = 0.844$, $Re_c = 0.17 \times 10^6$

Variable	Nominal value	w_i	$\partial C_p / \partial v_i$	$(w_i \partial C_p / \partial v_i)^2 \times 10^4$
Counter time	486 μsec^a	$\pm 3 \mu\text{sec}$	4.02×10^{-3}	1.454
p_1	40 torr	$\pm 0.5 \text{ torr}$	2.51×10^{-2}	1.575
Δy_r (eq. (6))	2.14 cm	$\pm 0.04 \text{ cm}$	4.693×10^{-1}	3.523
OVS (eq. (6))	1.048 mV/cm	$\pm 0.02 \text{ mV/cm}$	9.5850×10^{-1}	3.675
TCF (eq. (6))	32.69 torr/mV	$\pm 0.65 \text{ torr/mV}$	3.072×10^{-2}	3.988
T_1	299 K	$\pm 1 \text{ K}$	1.81×10^{-3}	0.131
γ	1.4	± 0.05	9.46×10^{-2}	0.224
				14.570

^a For 0.3048-m interval.

Thus, from equation (B1)

$$w_{C_p} = \pm \sqrt{14.57 \times 10^{-4}} = \pm 0.0382$$

The value of C_p computed using the nominal values in table 1 is -0.4504.
Thus, for the typical run

$$C_p = -0.4504 \pm 0.0382$$

REFERENCES

1. Alexander, W. K.; and Griffin, S. A.: Design Study of Basic Models for Use in the Proposed 8 by 10 Foot High Reynolds Number Transonic Wind Tunnel (HIRT) at Arnold Engineering Development Center. AIAA Paper 74-82, AIAA 12th Aerospace Sciences Meeting, Washington, D.C., Jan. 30-Feb. 1, 1974.
2. Kamchi, Jerome S.: National Aeronautical Facilities Program - the Need, the Facilities, and the Impact. AIAA Paper 74-79, AIAA 12th Aerospace Sciences Meeting, Washington, D.C., Jan. 30-Feb. 1, 1974.
3. Polhamus, E. C.; Kilgore, R. A.; Adcock, J. B.; and Ray, E. J.: The Langley Cryogenic High Reynolds Number Wind-Tunnel Program. Astronaut. & Aeronaut., vol. 12, no. 10, Oct. 1974, pp. 30-40.
4. Geiger, S. W.; Mautz, C. N.; and Hollyer, R. N., Jr.: The Shock Tube as an Instrument for the Investigation of Transonic and Supersonic Flow Patterns. Engineering Research Institute Report, Project M720-4, Univ. of Michigan, 1949.
5. Griffith, Wayland: Shock-Tube Studies of Transonic Flow over Wedge Profiles. J. Aeronaut. Sci., vol. 19, no. 4, Apr. 1952, pp. 249-257.
6. Ruetenik, J. Ray; and Whitmer, Emmett A.: Transient Aerodynamics of Two-Dimensional Airfoils. WADC Technical Report 54-368, pt. 2, Wright Air Development Center, Wright-Patterson Air Force Base, Ohio, Mar. 1958.
7. Varwig, R. L.; and Rosenman, L.: A 7-Foot-Diameter Shock Tube for Transonic and Supersonic Aerodynamic Testing. J. Spacecraft, vol. 3, no. 12, Dec. 1966, pp. 1809-1811.
8. Glass, I. I.; and Patterson, G. N.: A Theoretical and Experimental Study of Shock-Tube Flows. J. Aeronaut. Sci., vol. 22, no. 2, Feb. 1955, pp. 73-100.
9. Wilke, C. R.: A Viscosity Equation for Gas Mixtures. J. of Chem. Physics, vol. 18, no. 4, Apr. 1950, pp. 517-519.
10. Mirels, Harold: Shock Tube Test Time Limitation due to Turbulent-Wall Boundary Layer. AIAA J., vol. 2, no. 1, Jan. 1964, pp. 84-93.
11. Goethert, Bernhard H.: Transonic Wind Tunnel Testing. Pergamon Press, New York, 1961.
12. Murman, Earll M.; and Cole, Julian D.: Calculation of Plane Steady Transonic Flows. AIAA J., vol. 9, no. 1, Jan. 1971, pp. 114-121.
13. Murman, Earll M.: Analysis of Embedded Shock Waves Calculated by Relaxation Methods. AIAA J., vol. 12, no. 5, May 1974, pp. 626-633.

14. Wood, George P.; and Gooderum, Paul B.: Investigation with an Interferometer of the Flow Around a Circular-Arc Airfoil at Mach Numbers Between 0.6 and 0.9. NACA TN 2801, 1952.
15. DeRose, Charles E.: Trim Attitude, Lift and Drag of Apollo Command Module with Offset Center-of-Gravity Positions at Mach Numbers to 29. NASA TN D-5276, 1969.
16. Kline, S. J.; and McClintock, F.: Describing Uncertainties in Single-Sample Experiments. Mech. Eng., vol. 75, no. 1, Jan. 1953, pp. 3-8.

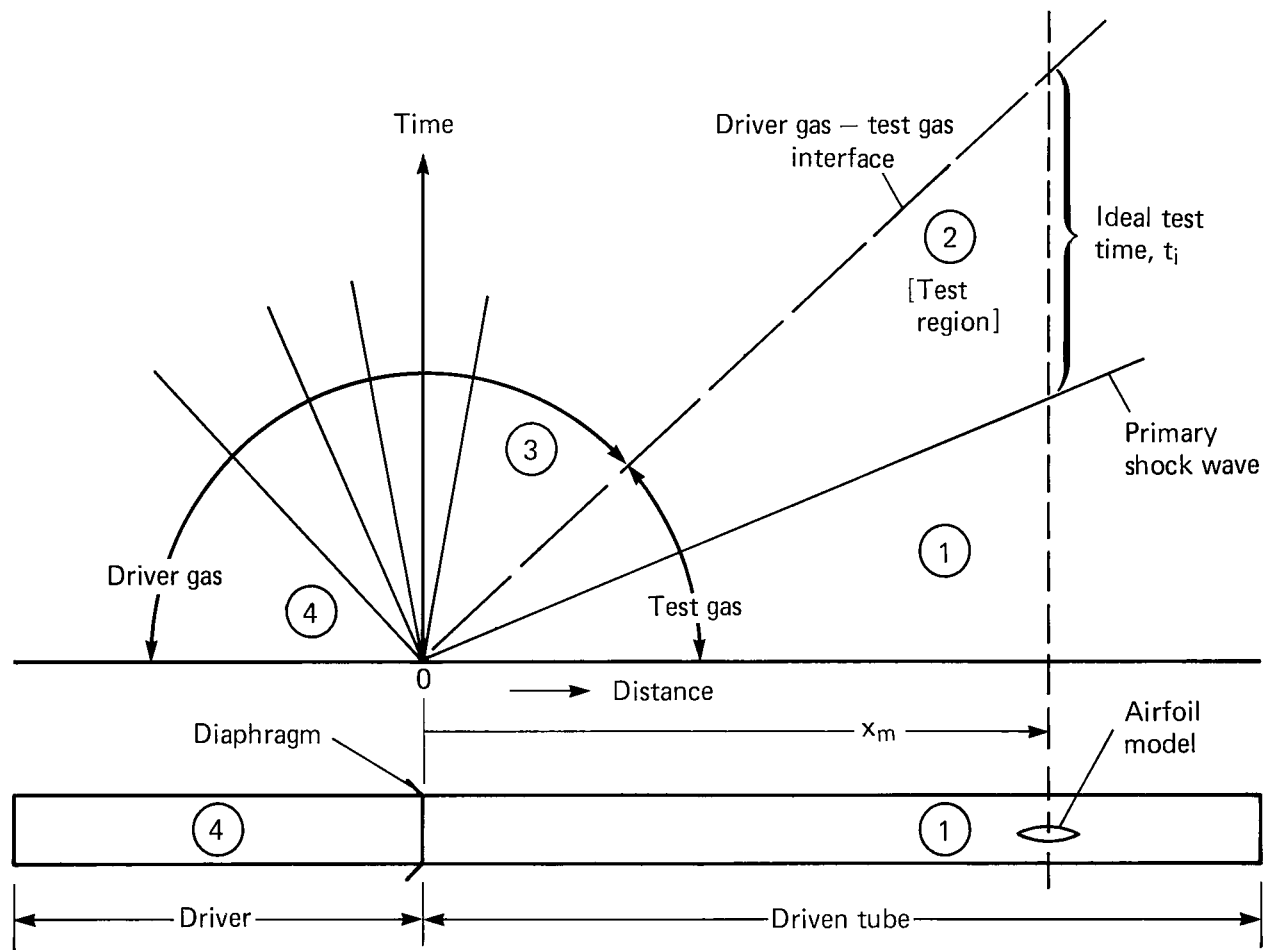
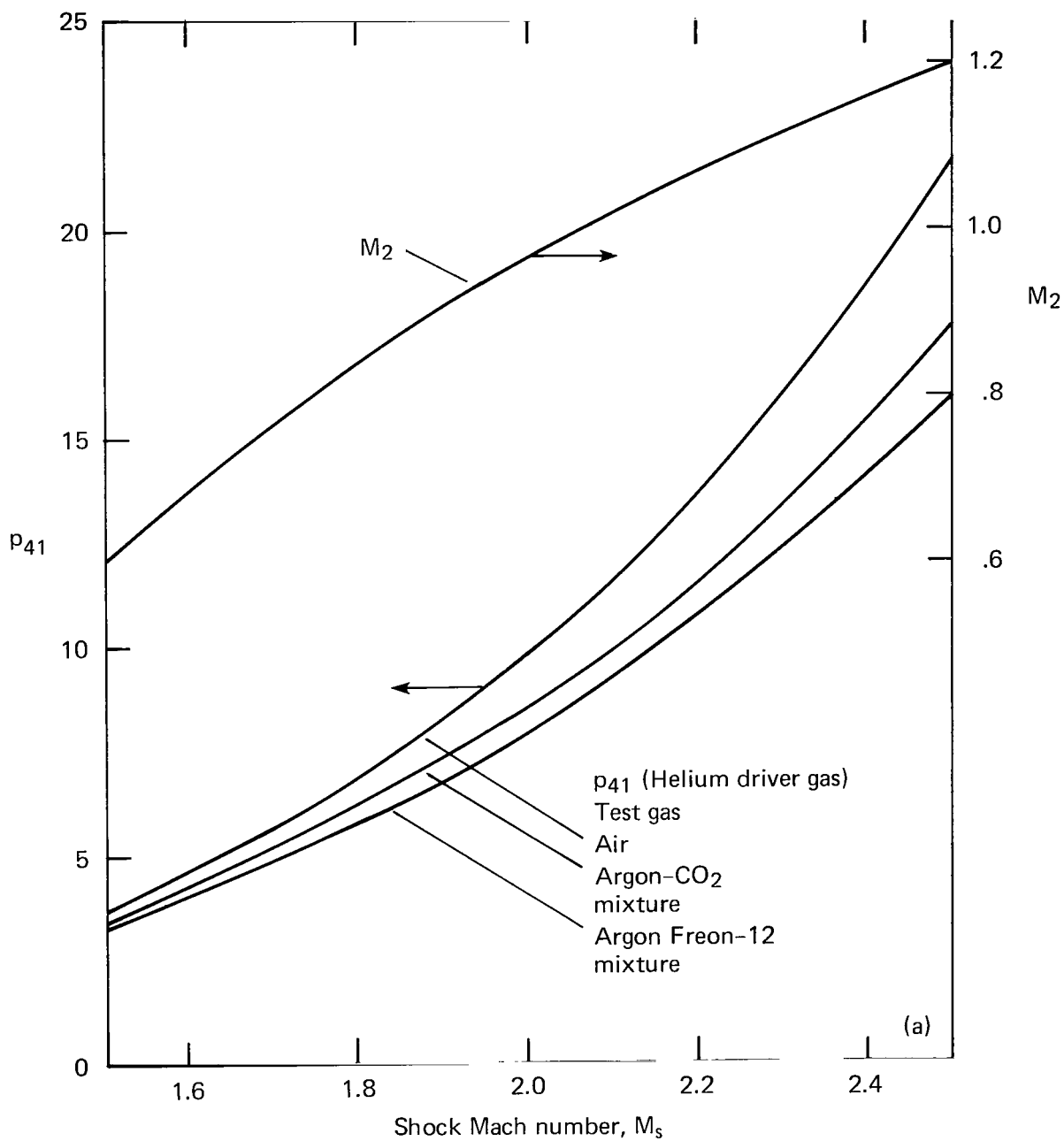
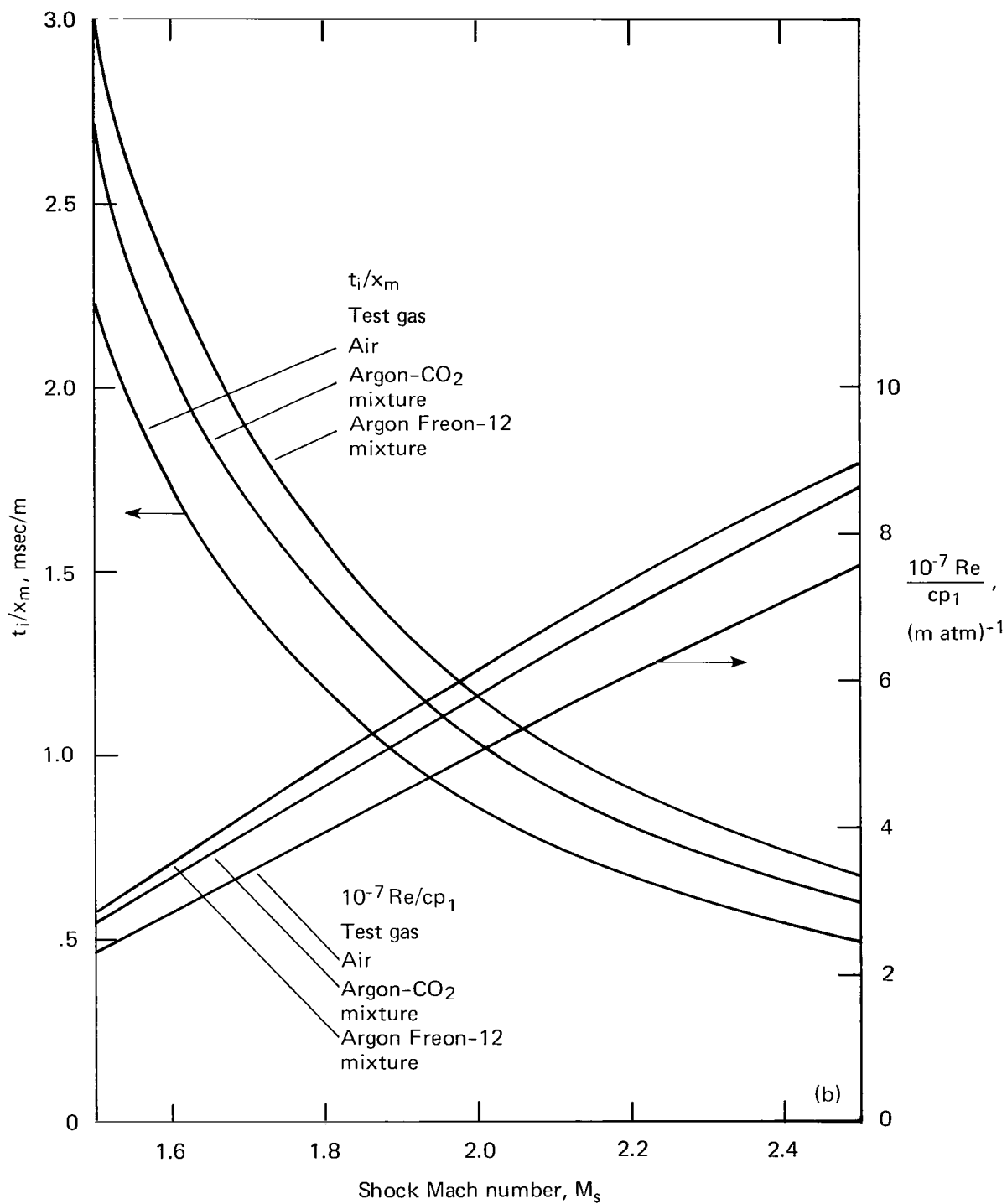


Figure 1.- Schematic diagram of a simple shock tube.



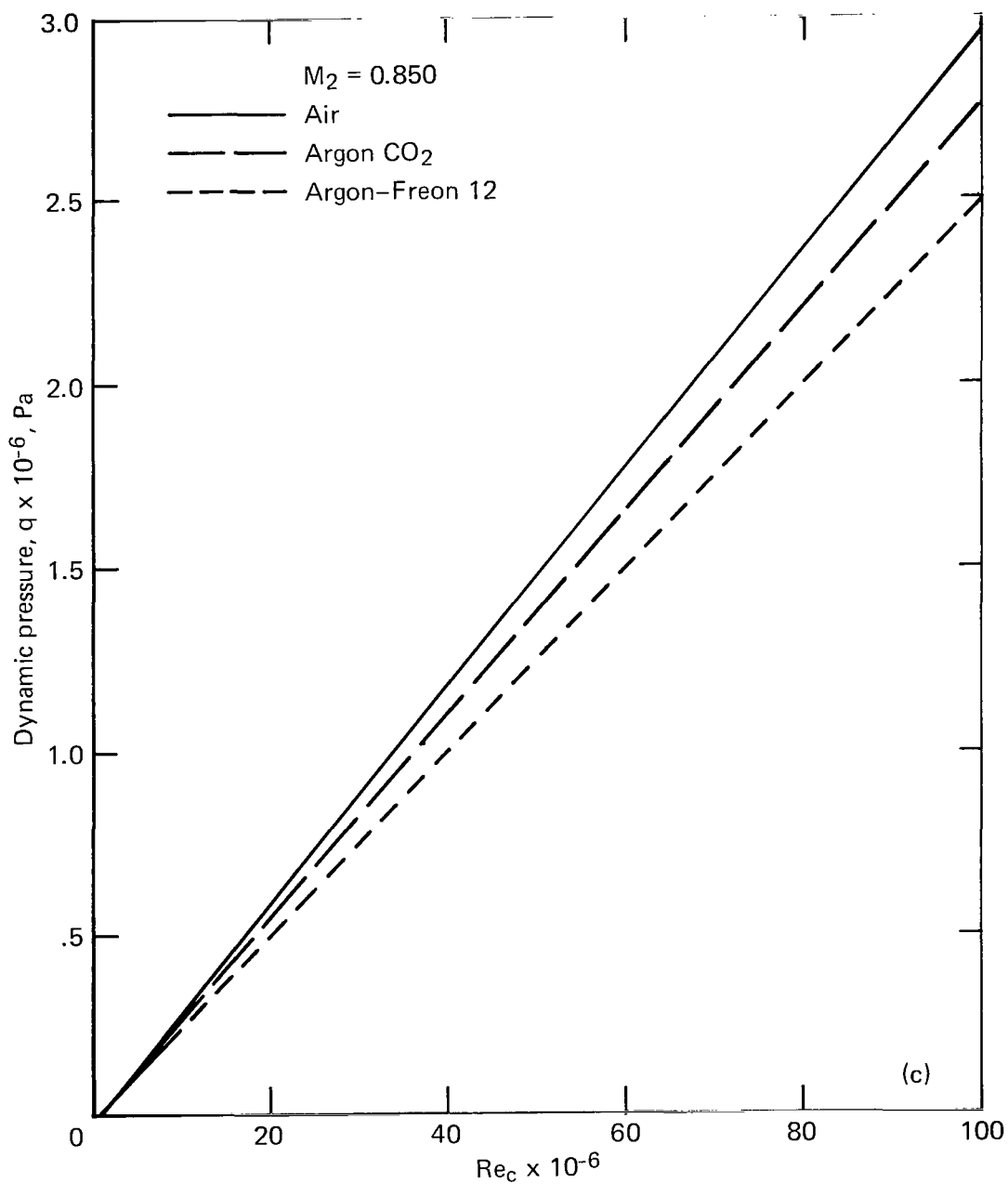
(a) M_2 and p_{41} vs shock Mach number.

Figure 2.- Shock-tube performance curves.



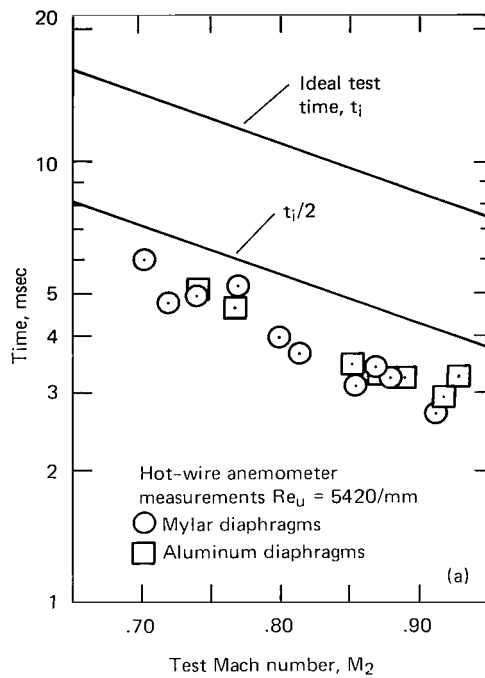
(b) t_i/x_m and Re/cp_1 vs shock Mach number.

Figure 2.- Continued.

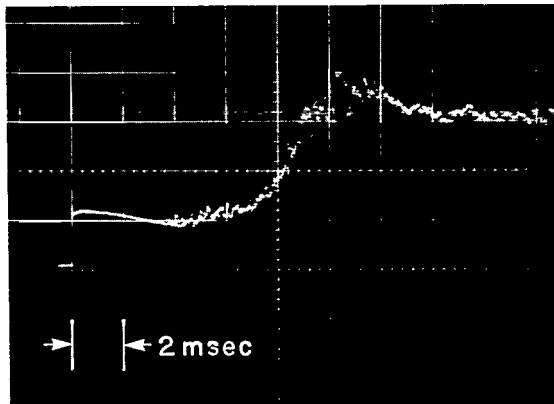


(c) Test region dynamic pressure vs chord Reynolds number, $c = 15.2$ cm.

Figure 2.- Concluded.

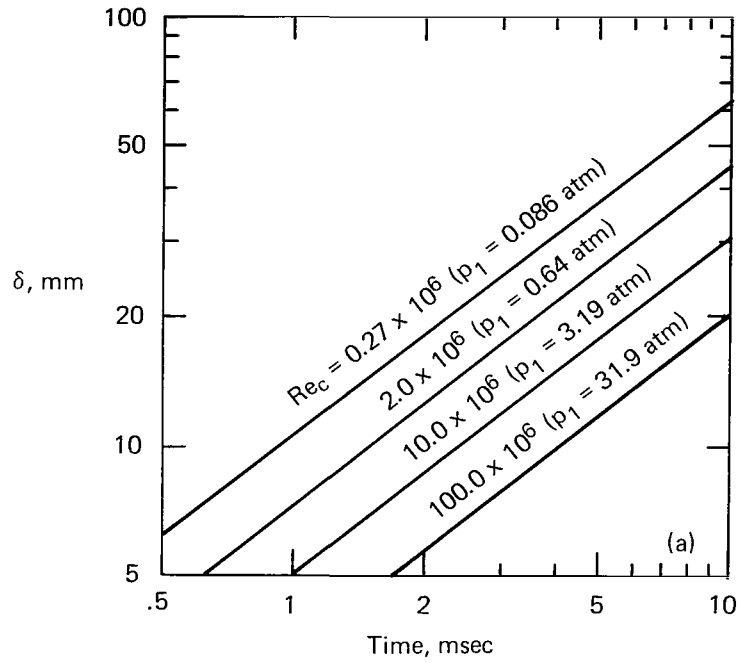


(a) Region 2 test time vs Mach number.

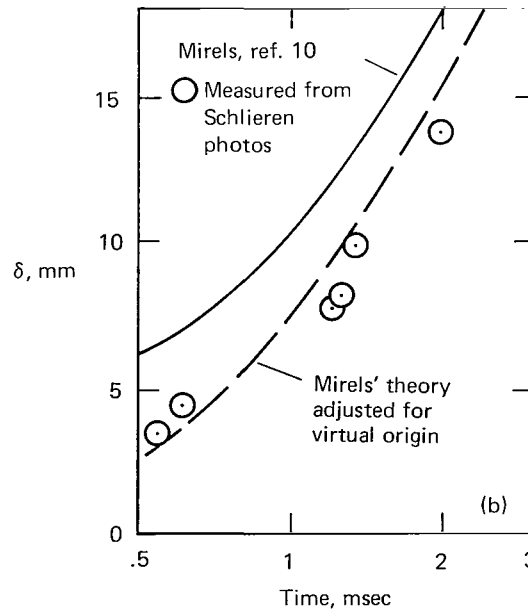


(b) Typical hot-wire response record.

Figure 3.- Shock-tube test time.



(a) Turbulent sidewall boundary-layer thickness vs time computed using reference 10; $c = 7.6$ cm, $M_2 = 0.850$.



(b) Comparison of growths of turbulent sidewall boundary layers; $M_2 = 0.870$, $Re_u = 4.89 \times 10^3/\text{mm}$.

Figure 4.- Turbulent sidewall boundary-layer thicknesses vs time.

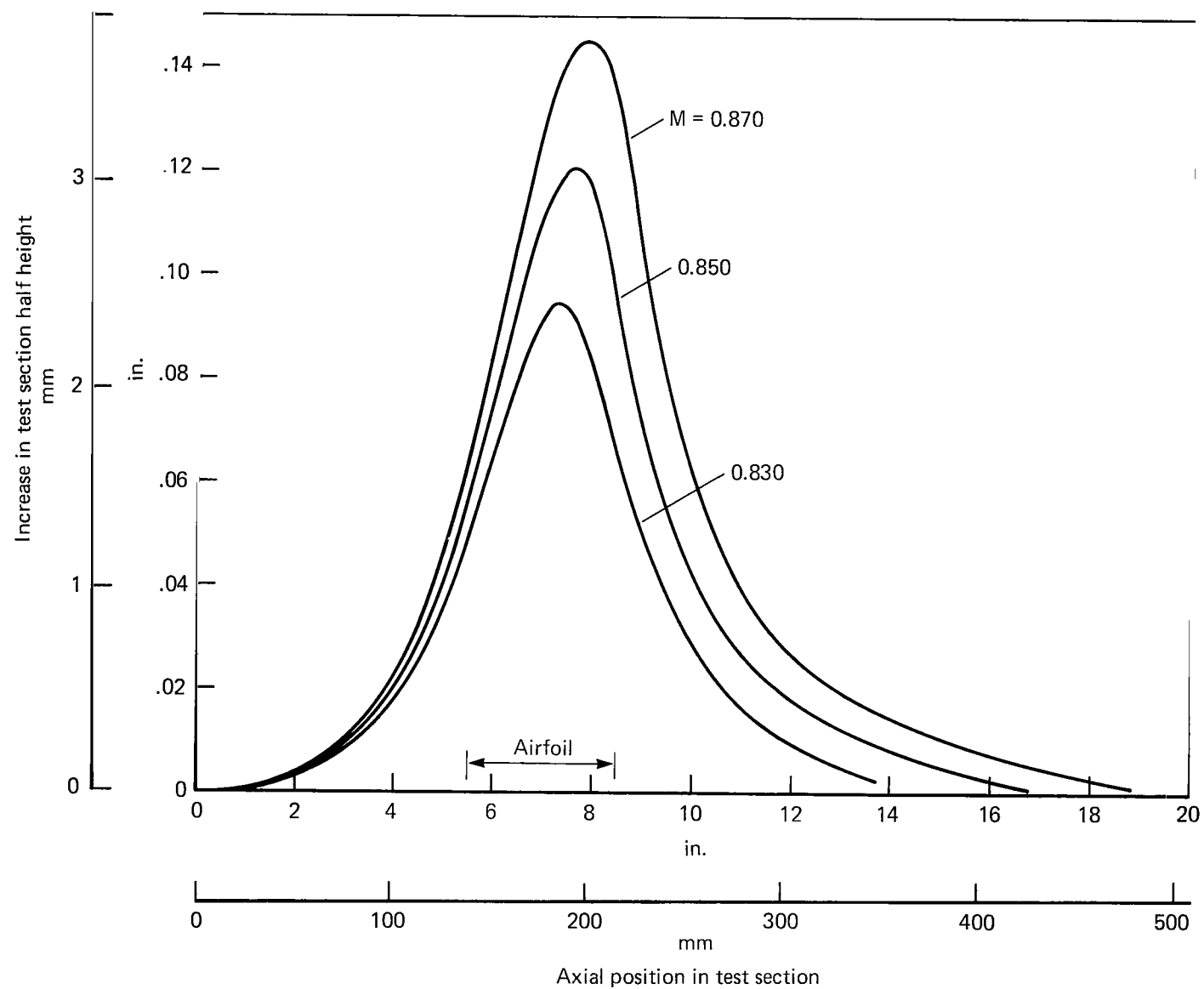


Figure 5.- Computed wall contours.

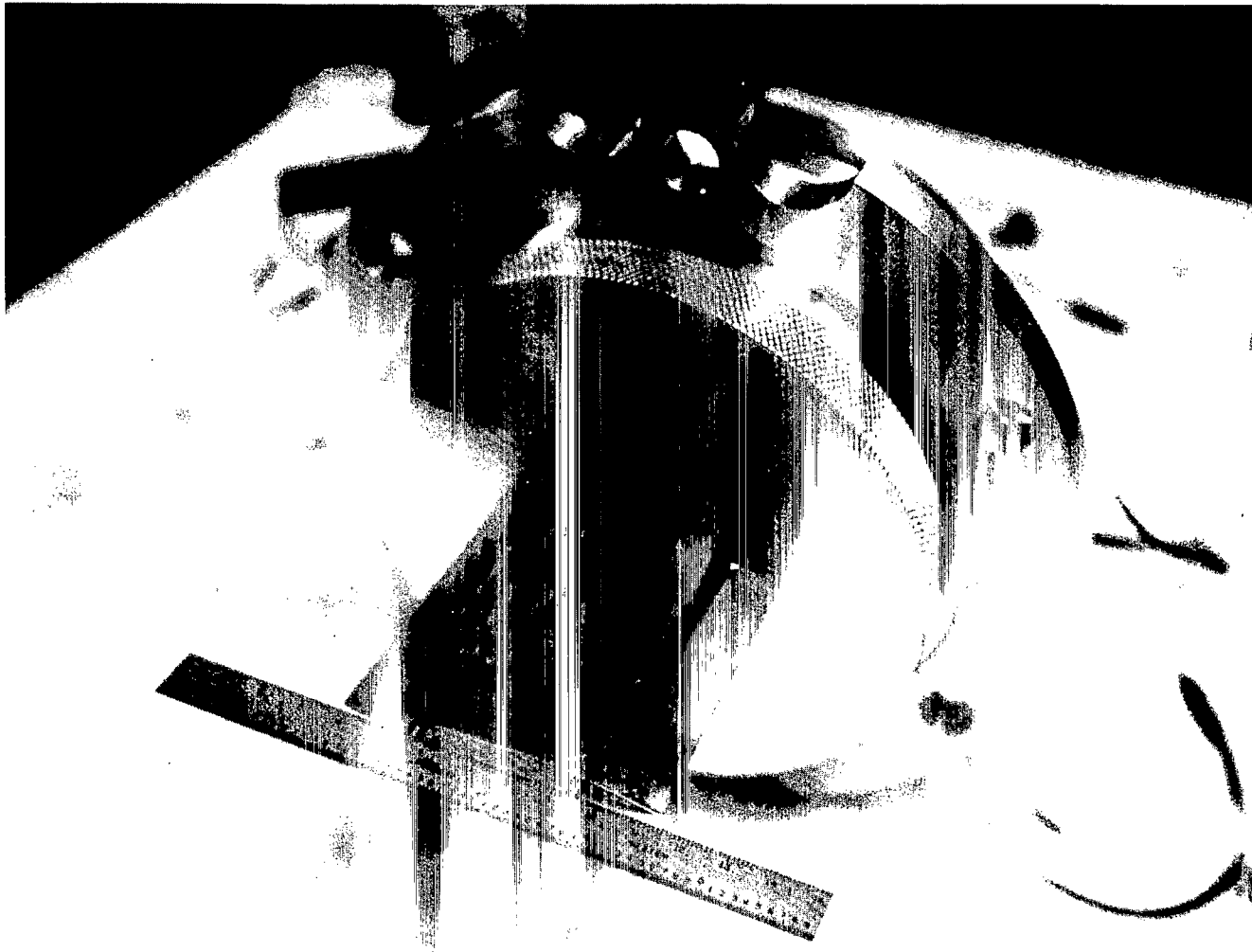


Figure 6.- Airfoil instrumented with pressure transducers.

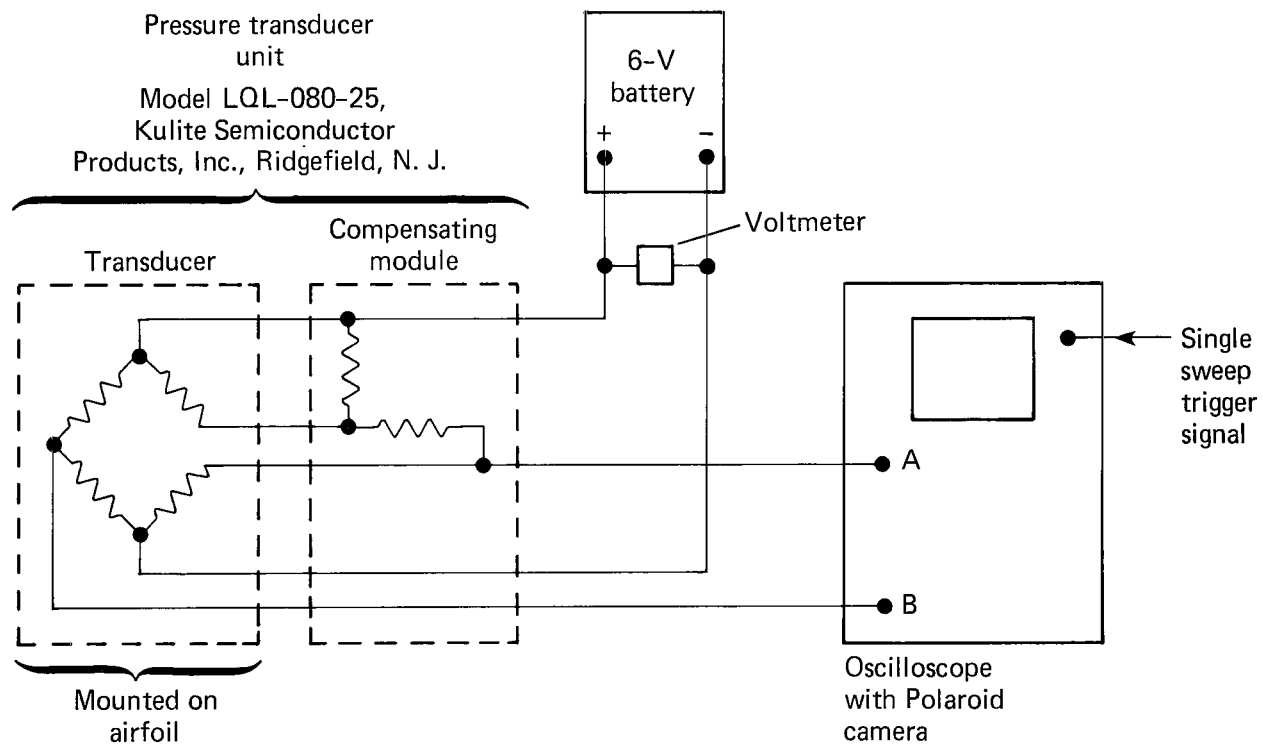
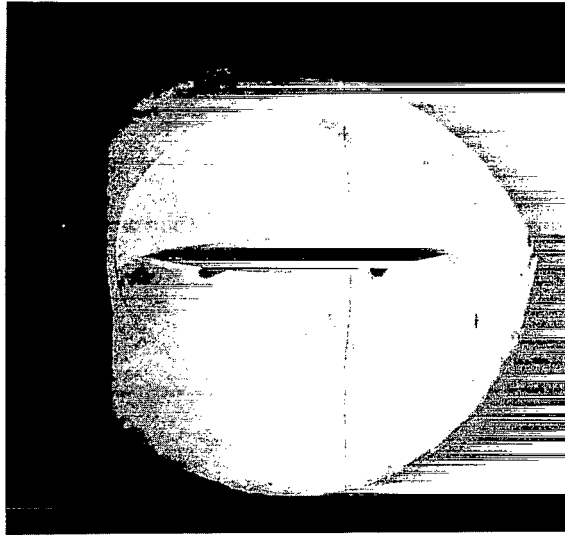
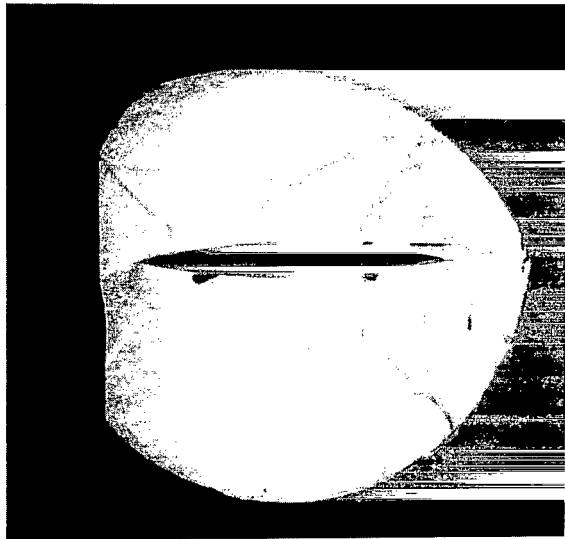


Figure 7.- Schematic diagram of pressure measurement system.

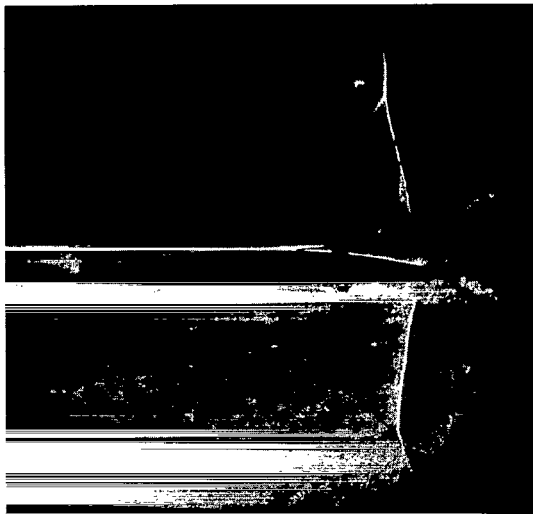


(a) $t' = 0.08$ msec.



(b) $t' = 0.5$ msec.

Figure 8.- Schlieren photos of airfoil flow development.



(c) $t' = 2.5$ msec, $M_2 = 0.85$, $Re_c = 0.27 \times 10^6$.



(d) $t' = 2.5$ msec, $M_2 = 0.85$, $Re_c = 2 \times 10^6$.

Figure 8.- Concluded.

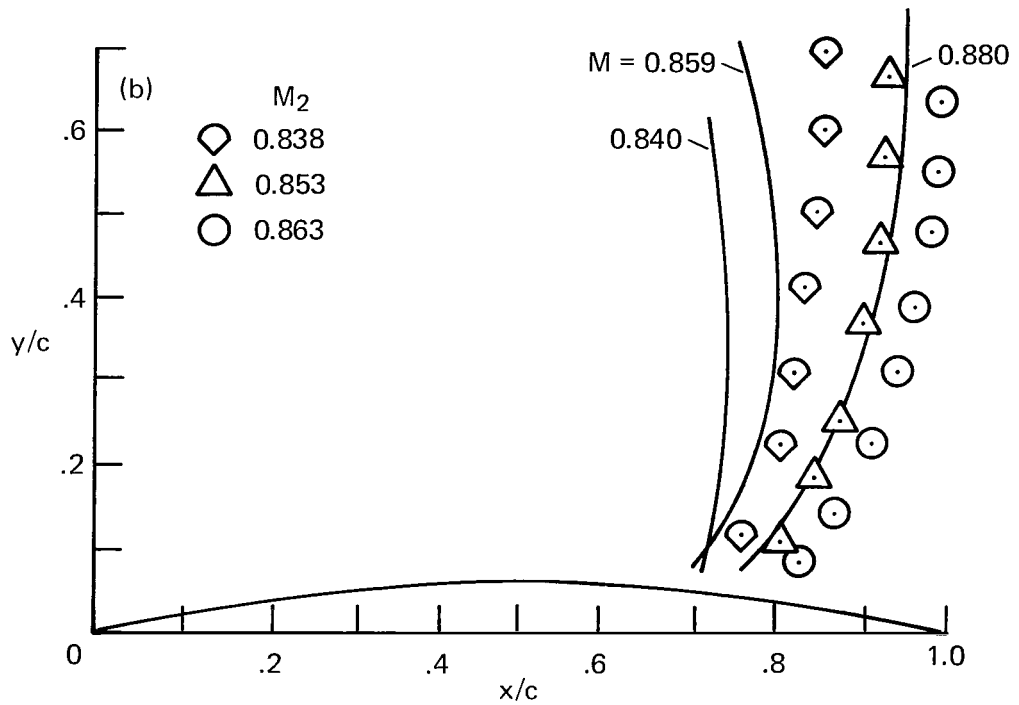
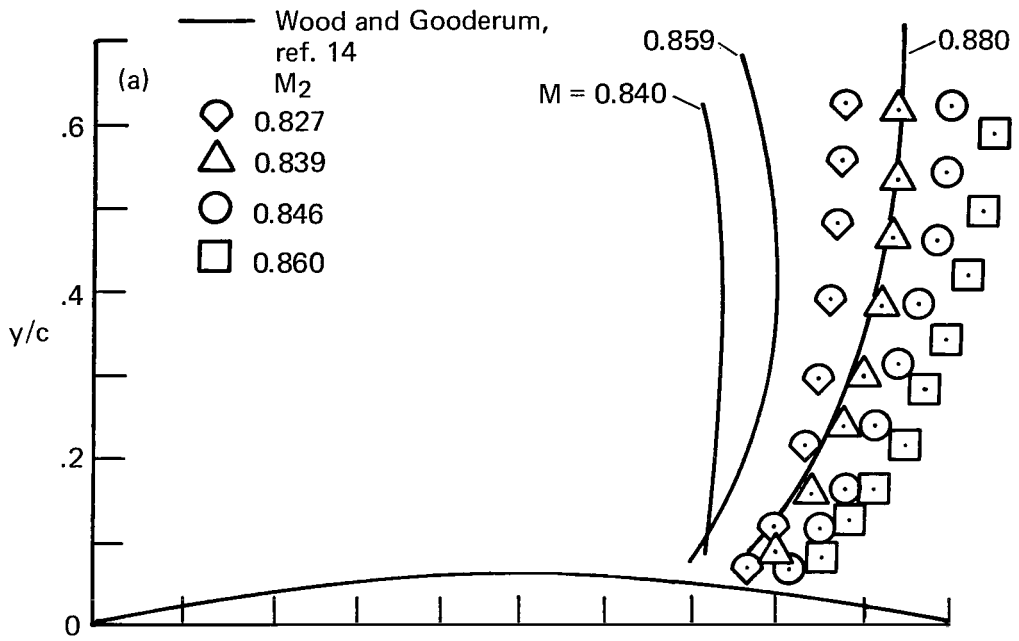
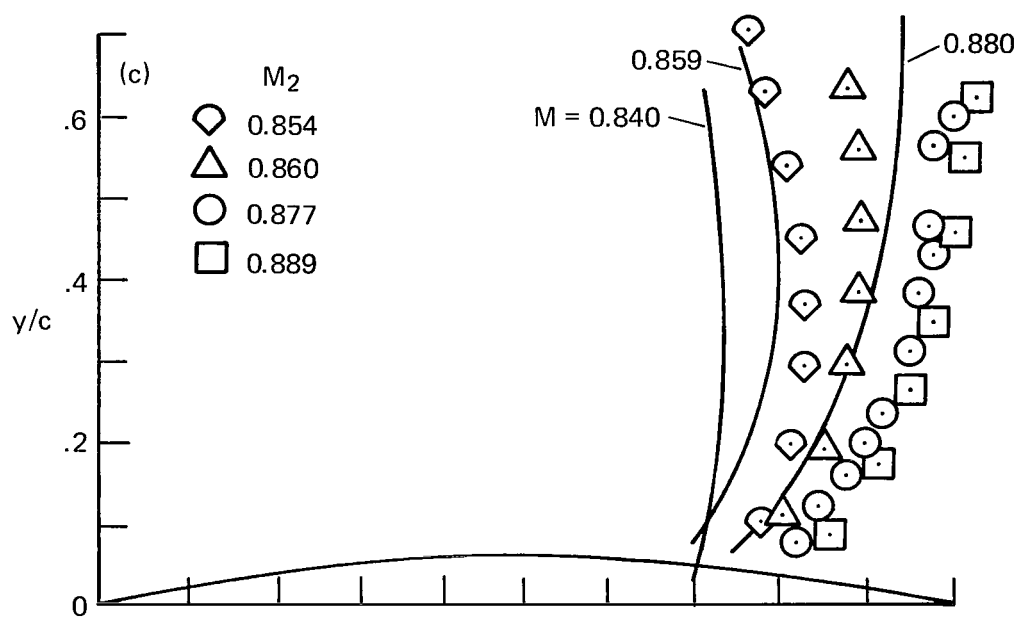
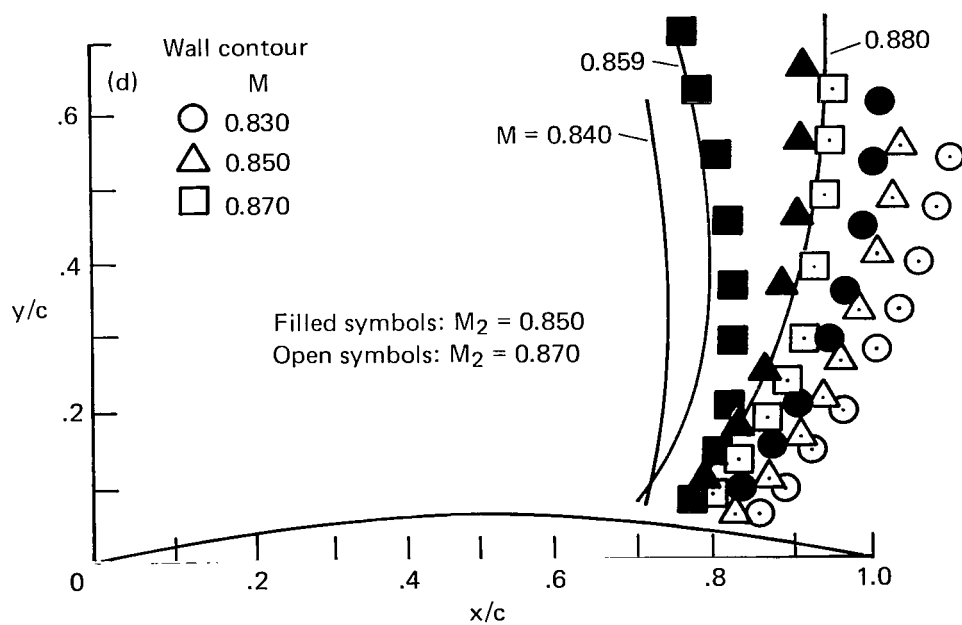


Figure 9.- Airfoil shock-wave profiles, turbulent airfoil boundary layer; $Re_c = 2 \times 10^6$. Symbols indicate present results.



(c) $M = 0.870$ wall contour.



(d) Results for three wall contours.

Figure 9.- Concluded.

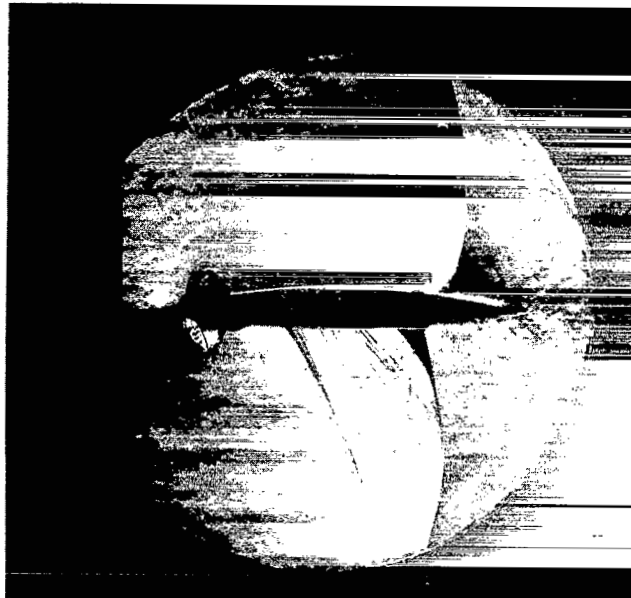
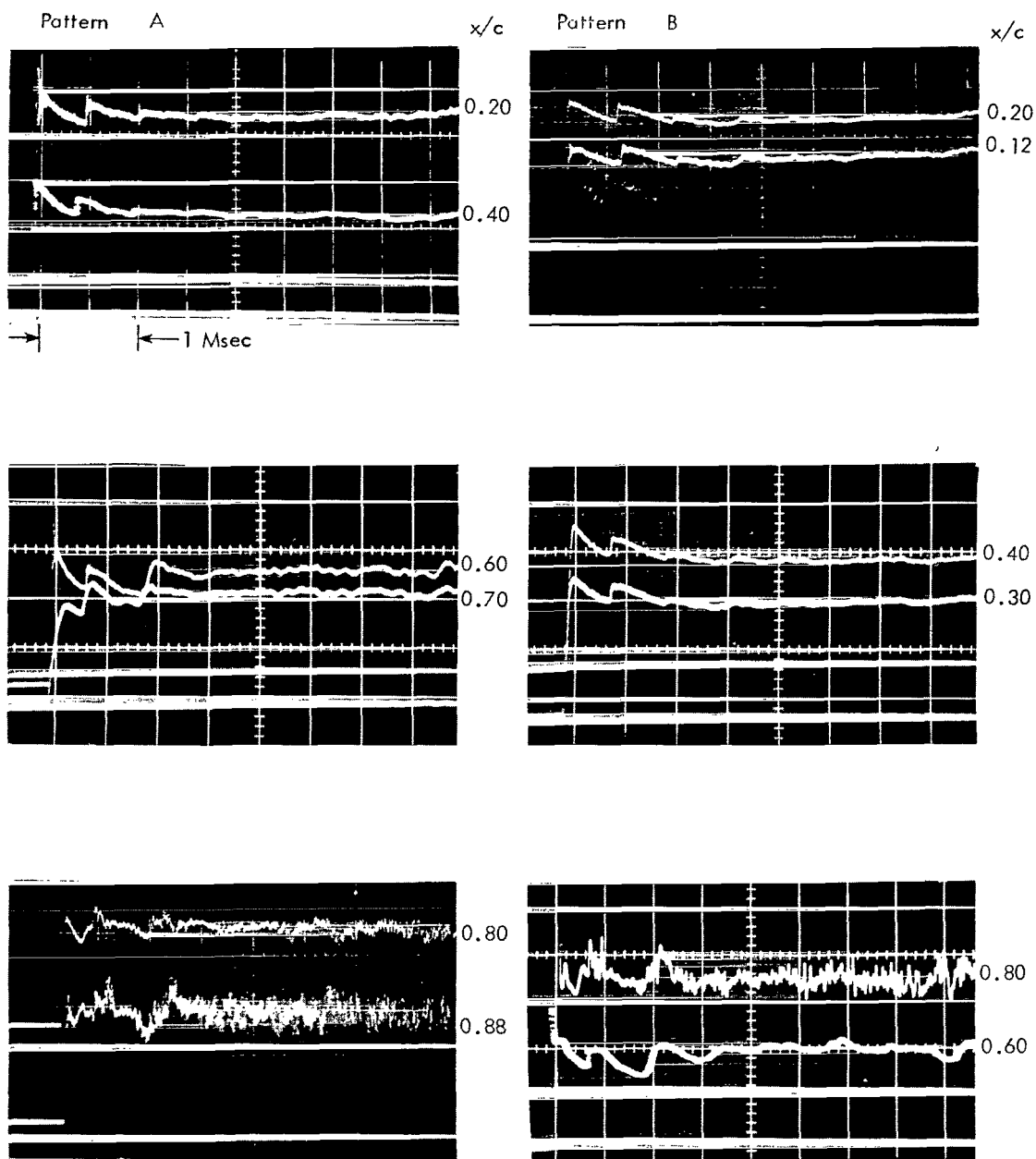
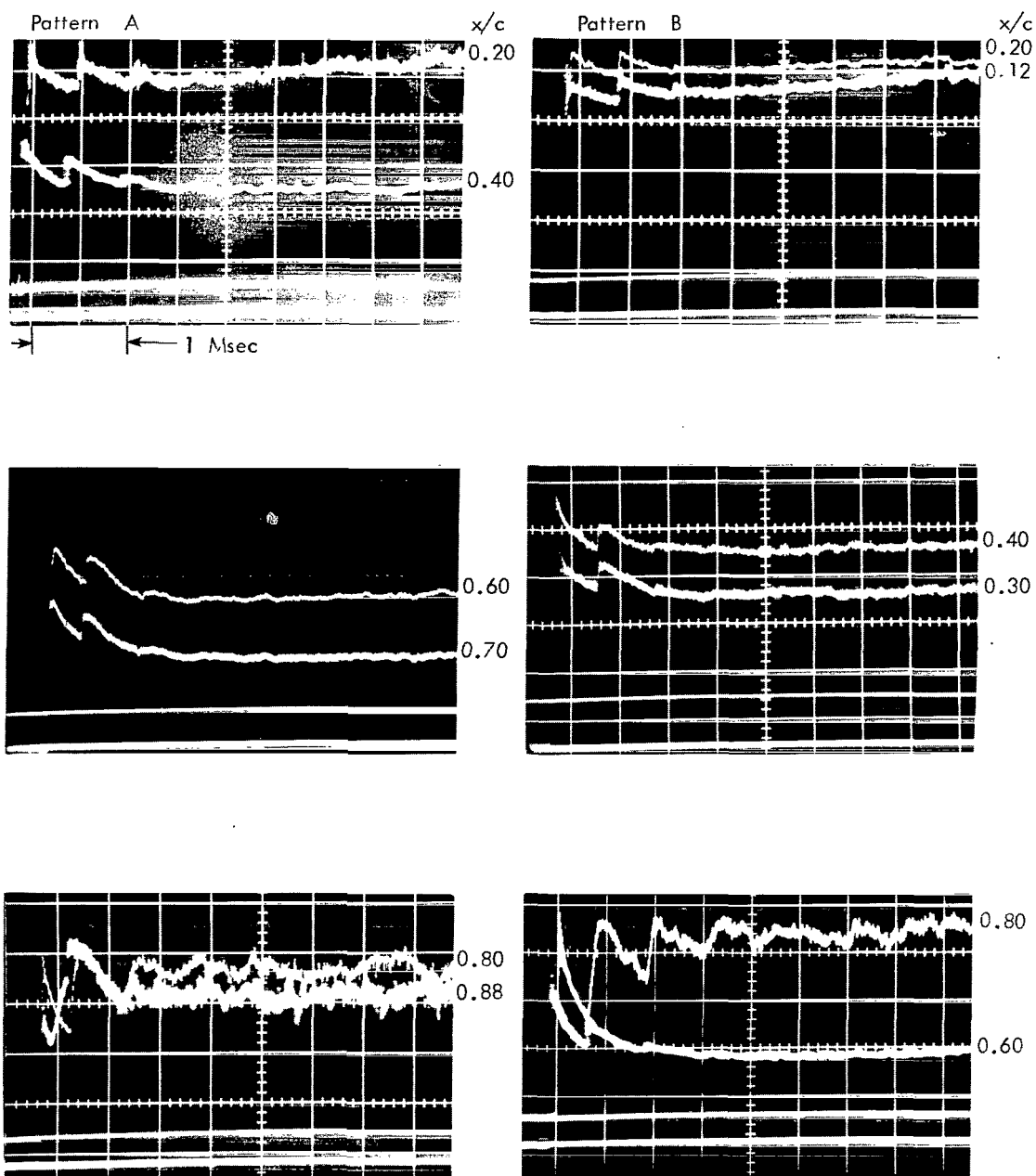


Figure 10.- Shock-wave profile. Upper airfoil surface smooth, lower surface roughened; $M_2 = 0.85$, $Re_c = 1.25 \times 10^6$.



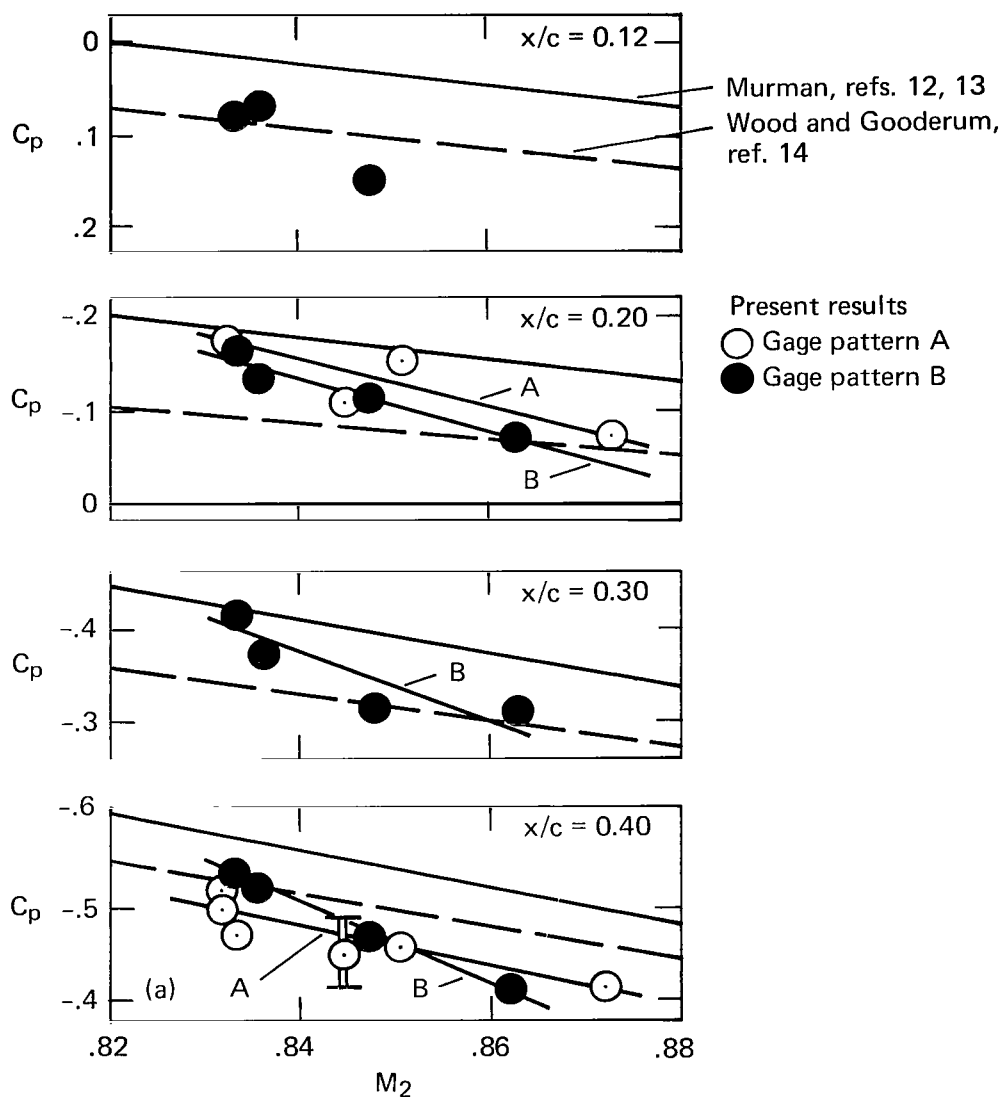
(a) Laminar airfoil boundary layer. Pattern A; $M_2 = 0.845$, $Re_c = 0.17 \times 10^6$. Pattern B; $M_2 = 0.836$, $Re_c = 0.17 \times 10^6$.

Figure 11.- Pressure transducer response records.



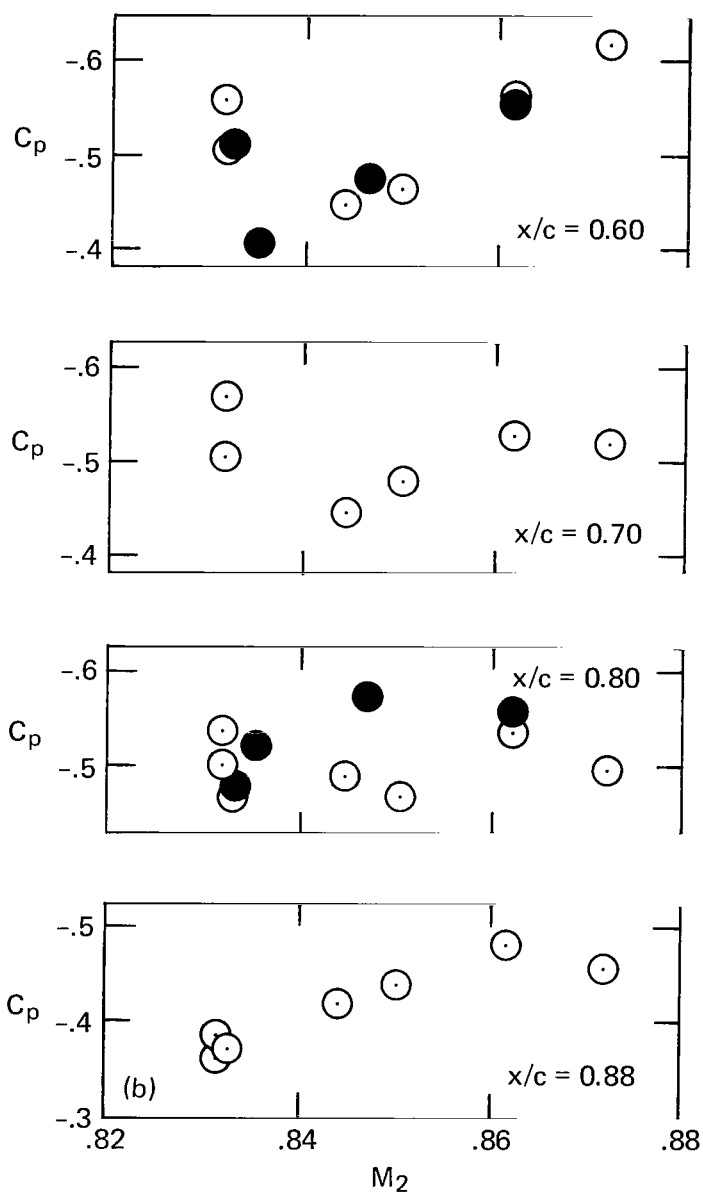
(b) Turbulent airfoil boundary layer. Pattern A; $M_2 = 0.850$, $Re_c = 2 \times 10^6$. Pattern B; $M_2 = 0.848$, $Re_c = 2 \times 10^6$.

Figure 11.- Concluded.



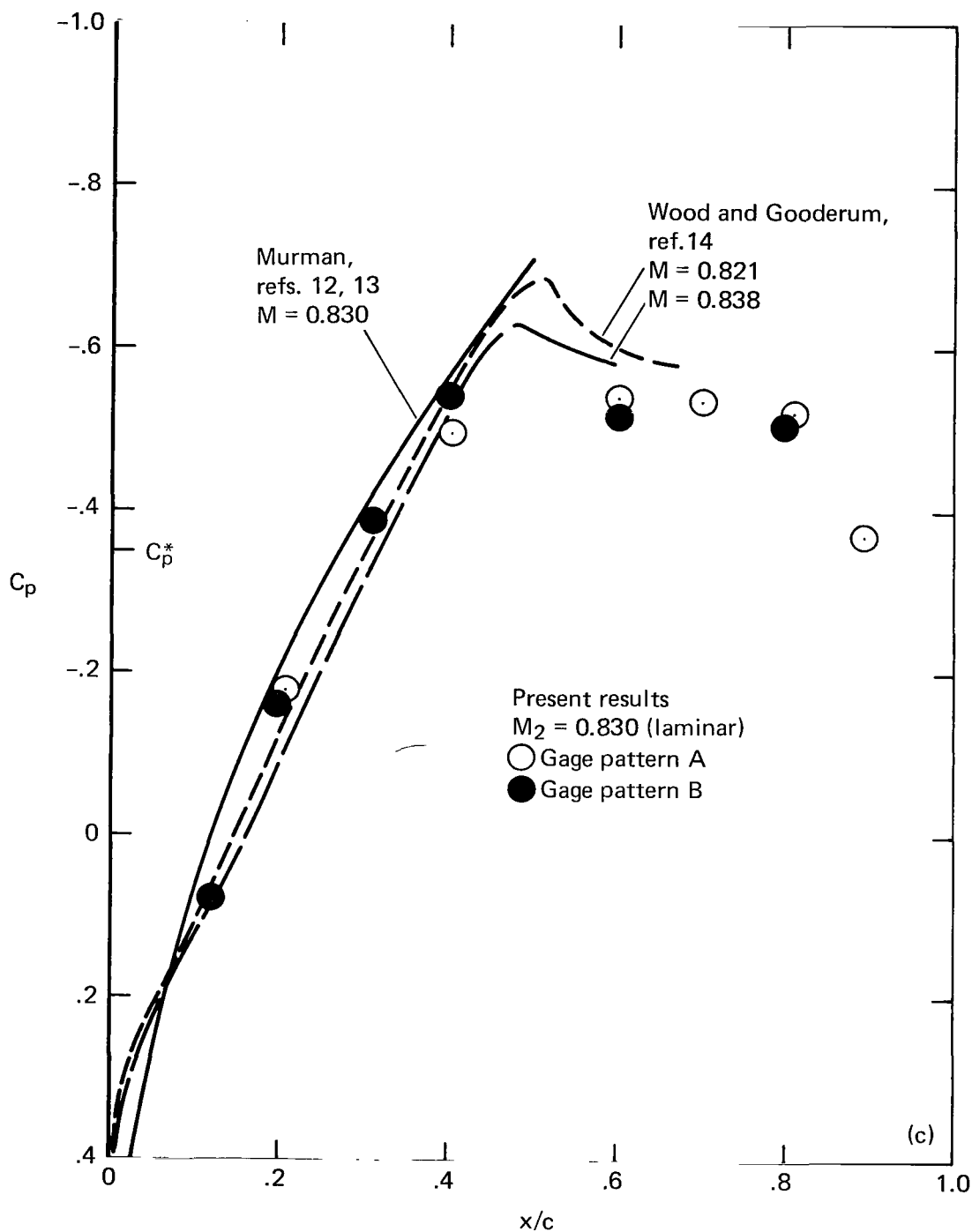
(a) Pressure coefficients vs M_2 . Present results for gage locations upstream of boundary-layer separation.
 $M = 0.830$ wall contour.

Figure 12.- Pressure coefficients for laminar airfoil boundary layer; $Re_c = 0.17 \times 10^6$.



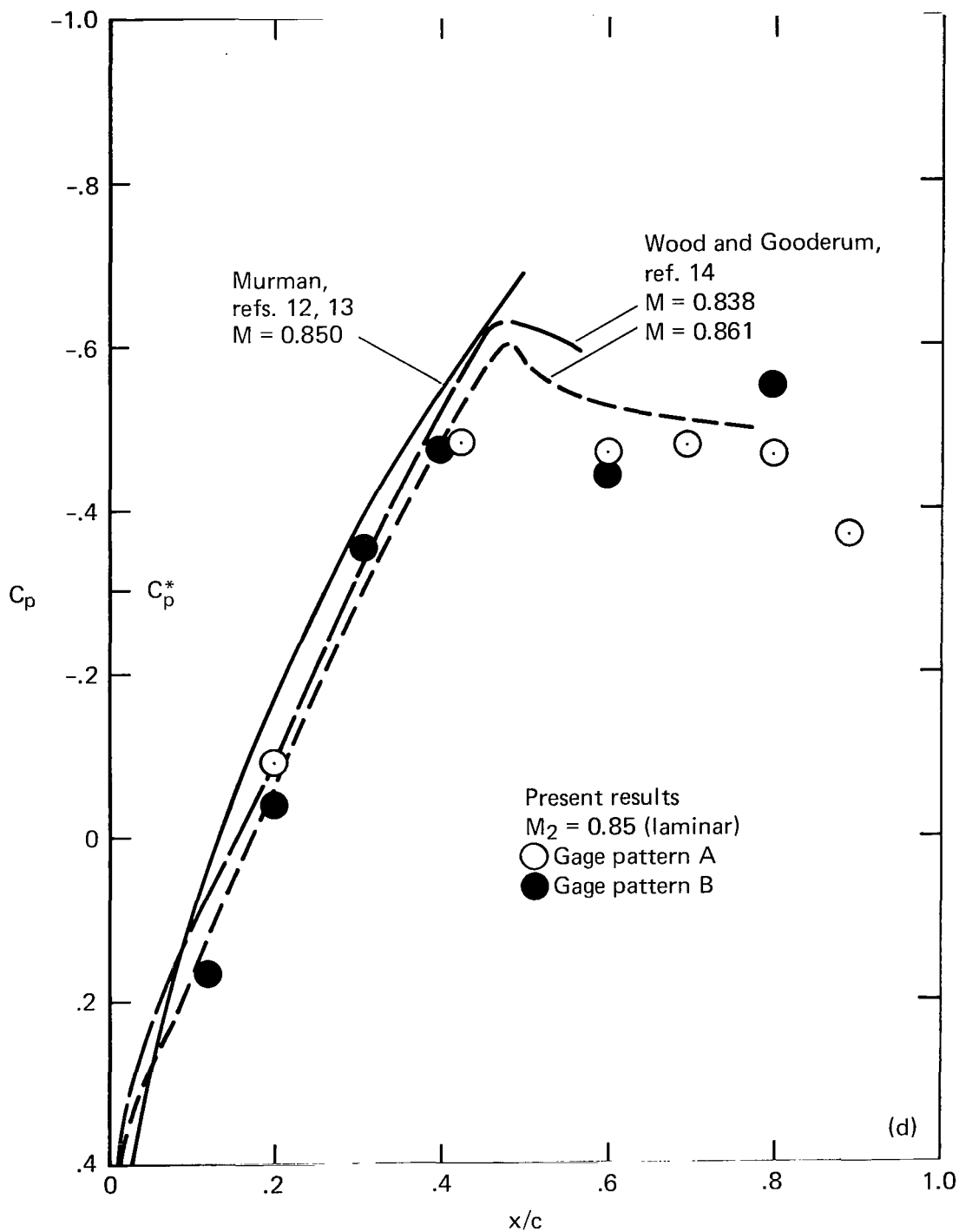
(b) Pressure coefficients vs M_2 . Present results for gage locations downstream of boundary-layer separation.

Figure 12.- Continued.



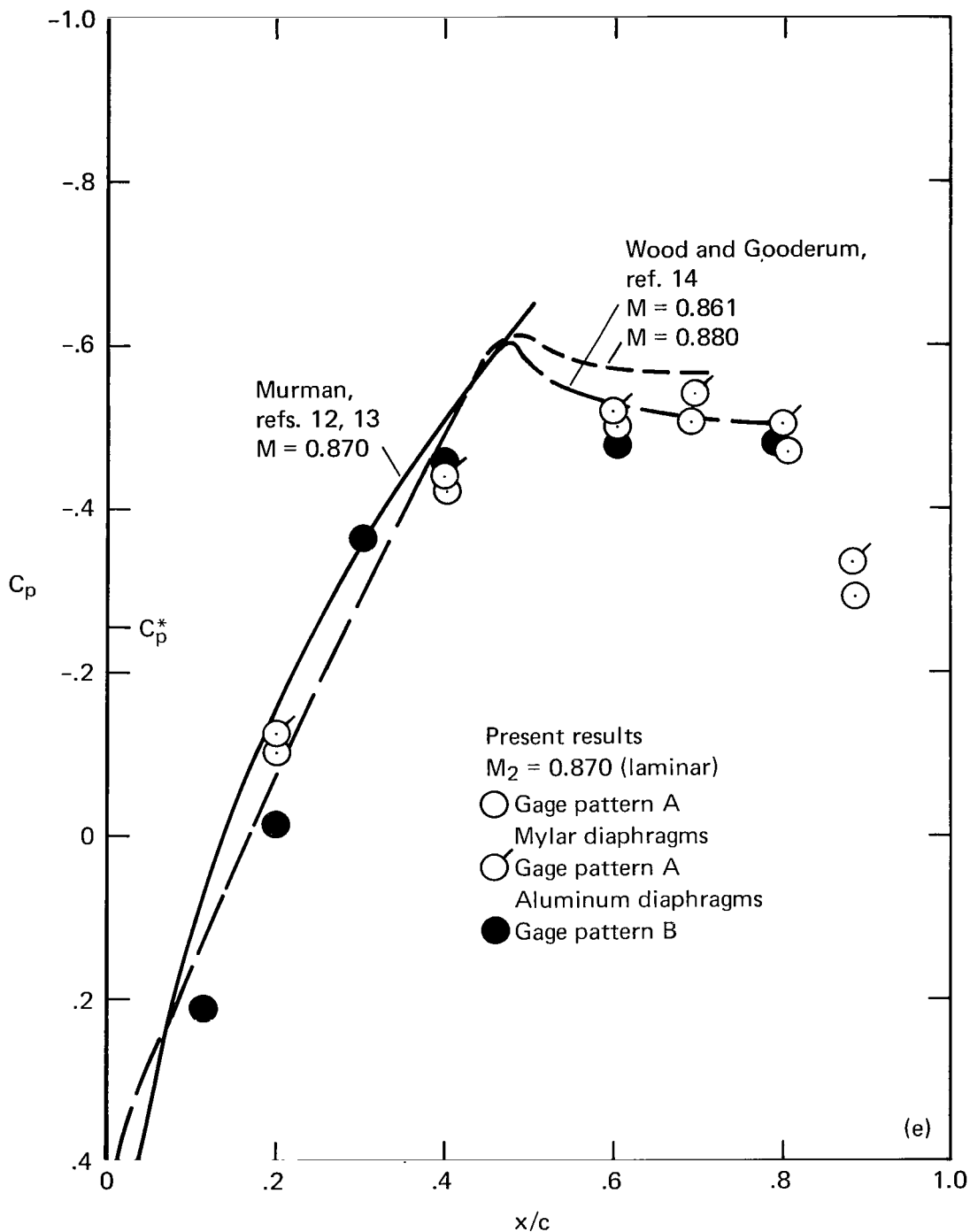
(c) Pressure coefficients vs chord position.
Present results; $M = 0.830$ wall contour.

Figure 12.- Continued.



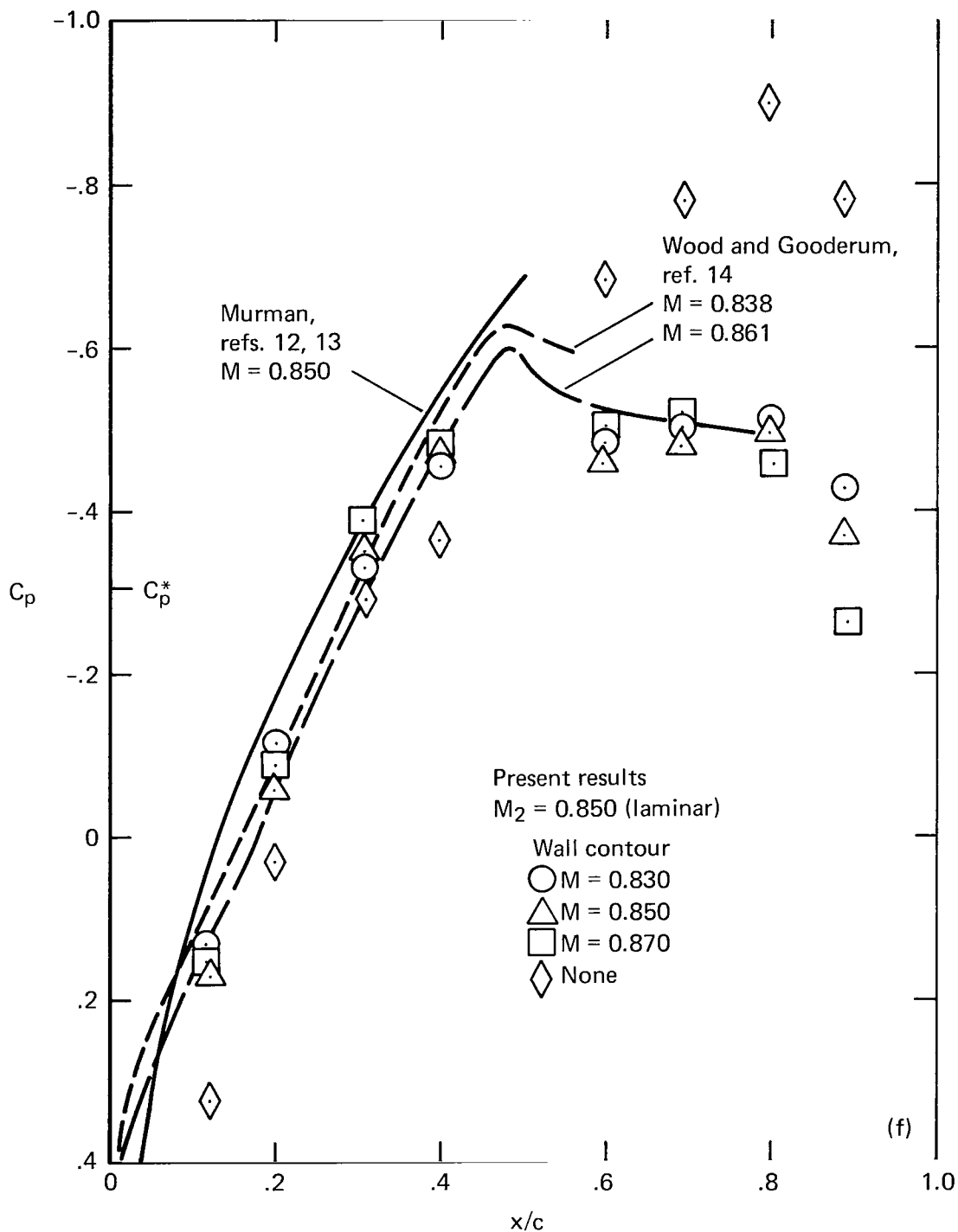
(d) Pressure coefficients vs chord position.
Present results; $M = 0.850$ wall contour.

Figure 12.- Continued.



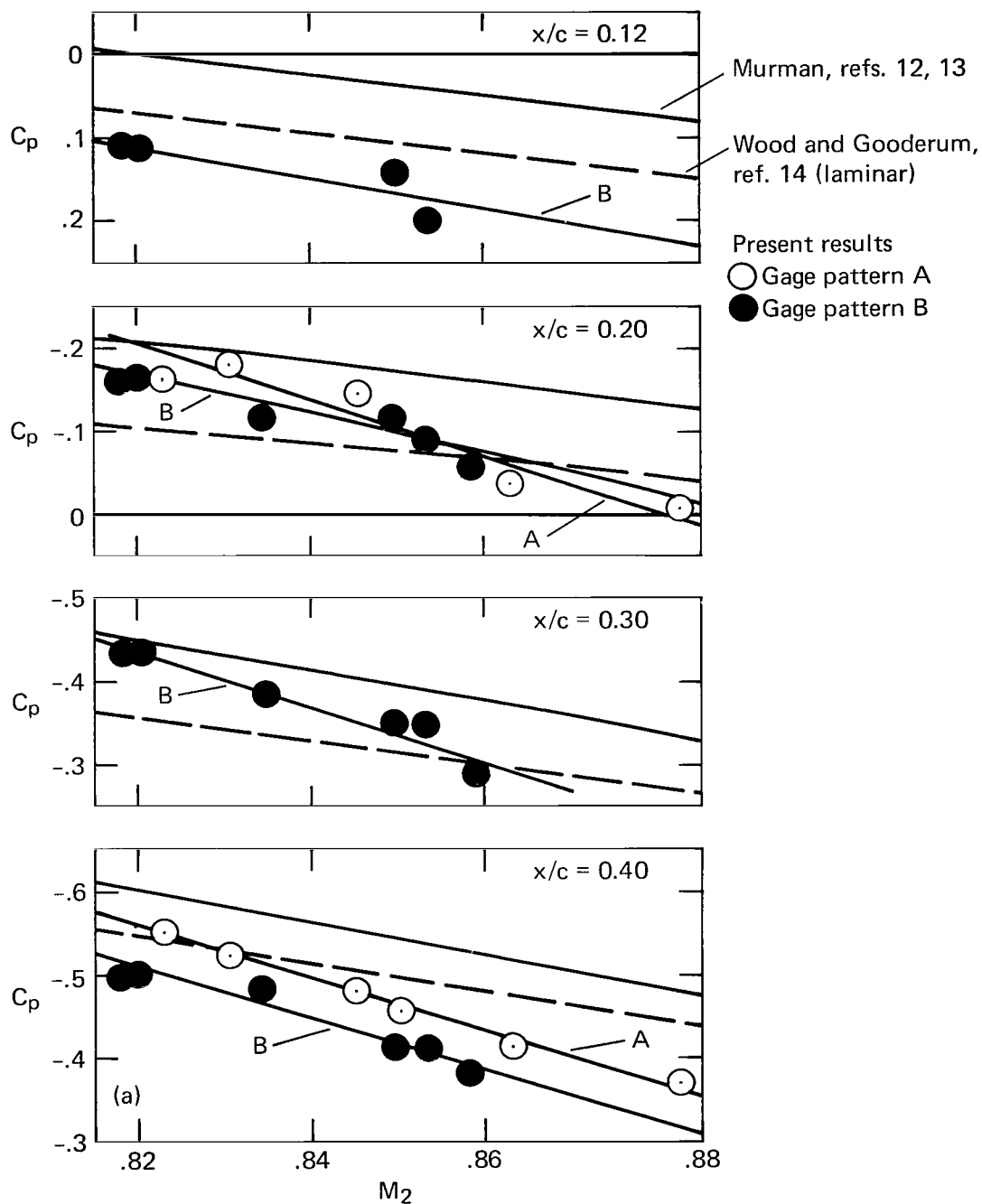
(e) Pressure coefficients vs chord position.
Present results; $M = 0.870$ wall contour.

Figure 12.- Continued.



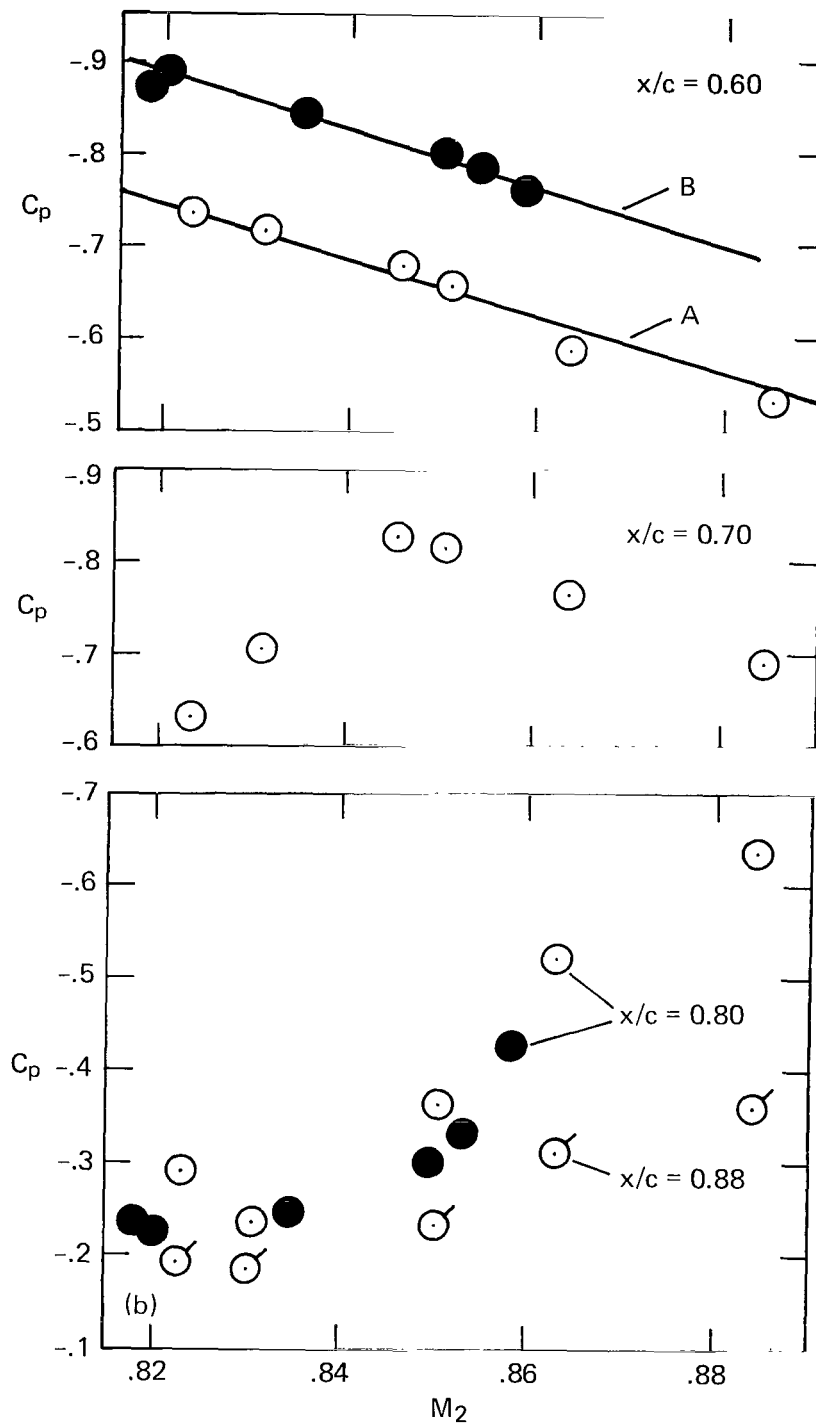
(f) Pressure coefficients vs chord position.

Figure 12.- Concluded.



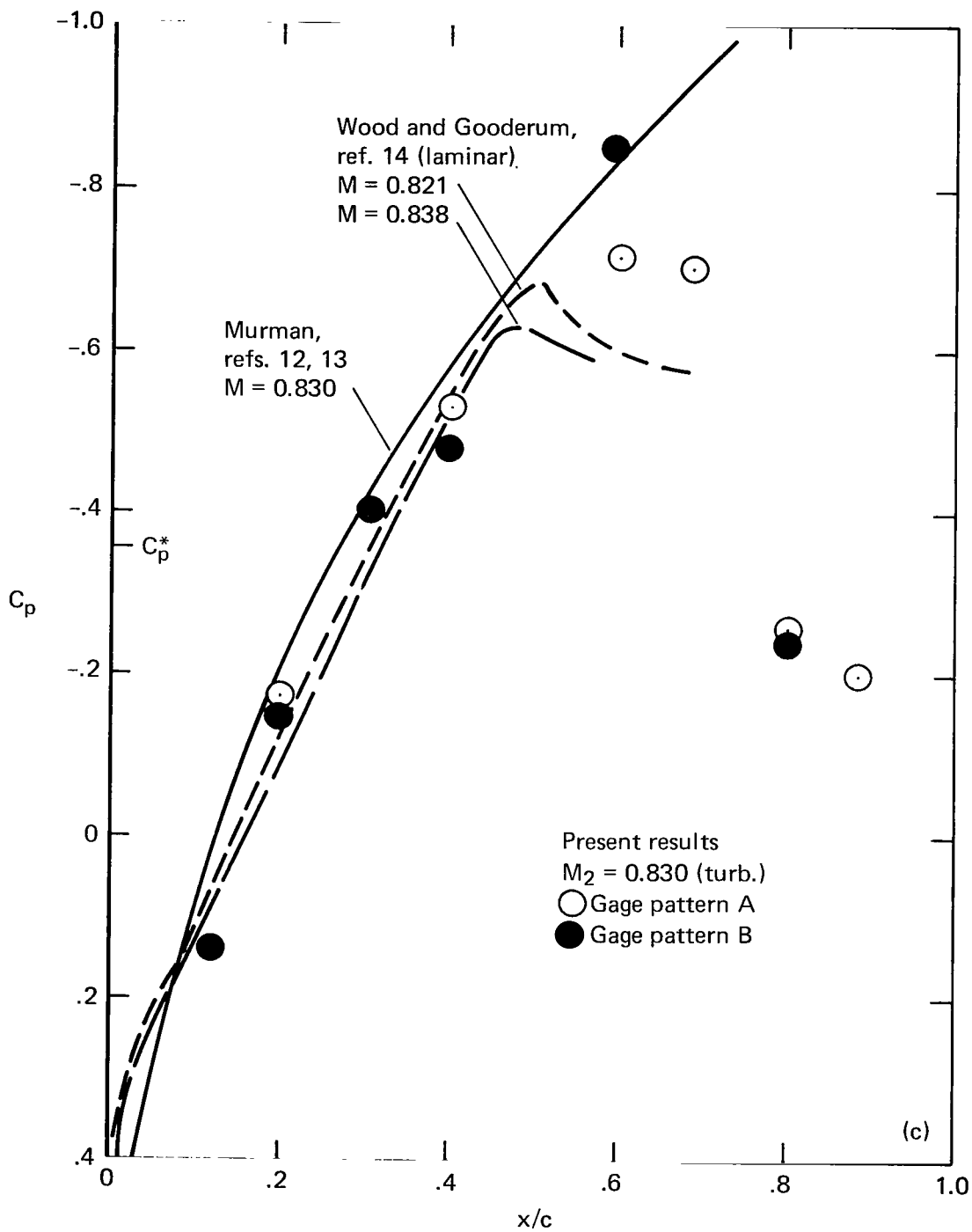
(a) Pressure coefficients vs M_2 . Present results;
 $M = 0.830$ wall contour.

Figure 13.- Pressure coefficients for turbulent airfoil
 boundary layer; $Re_c = 2 \times 10^6$.



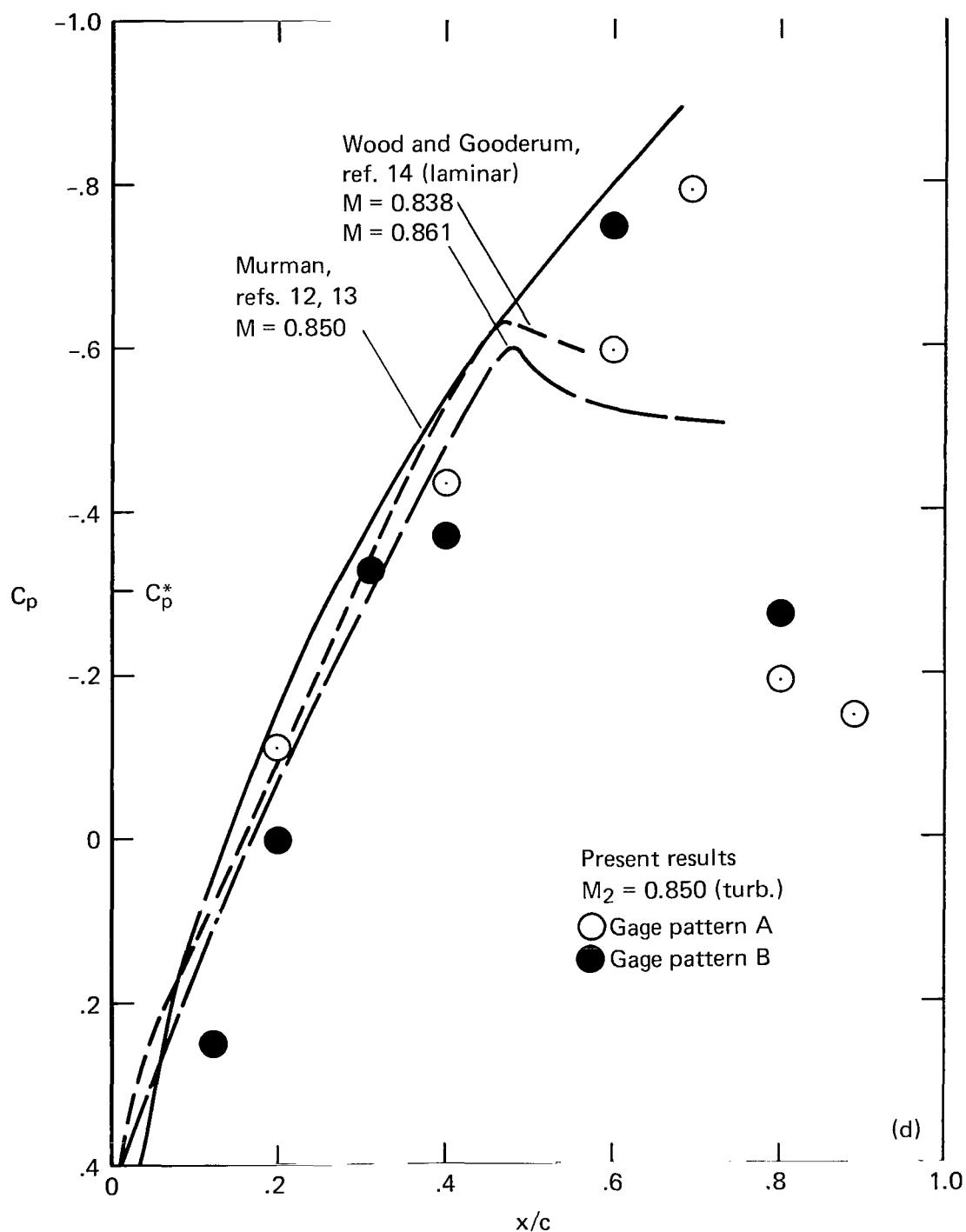
(b) Pressure coefficients vs M_2 . Present results;
 $M = 0.830$ wall contour.

Figure 13.- Continued.



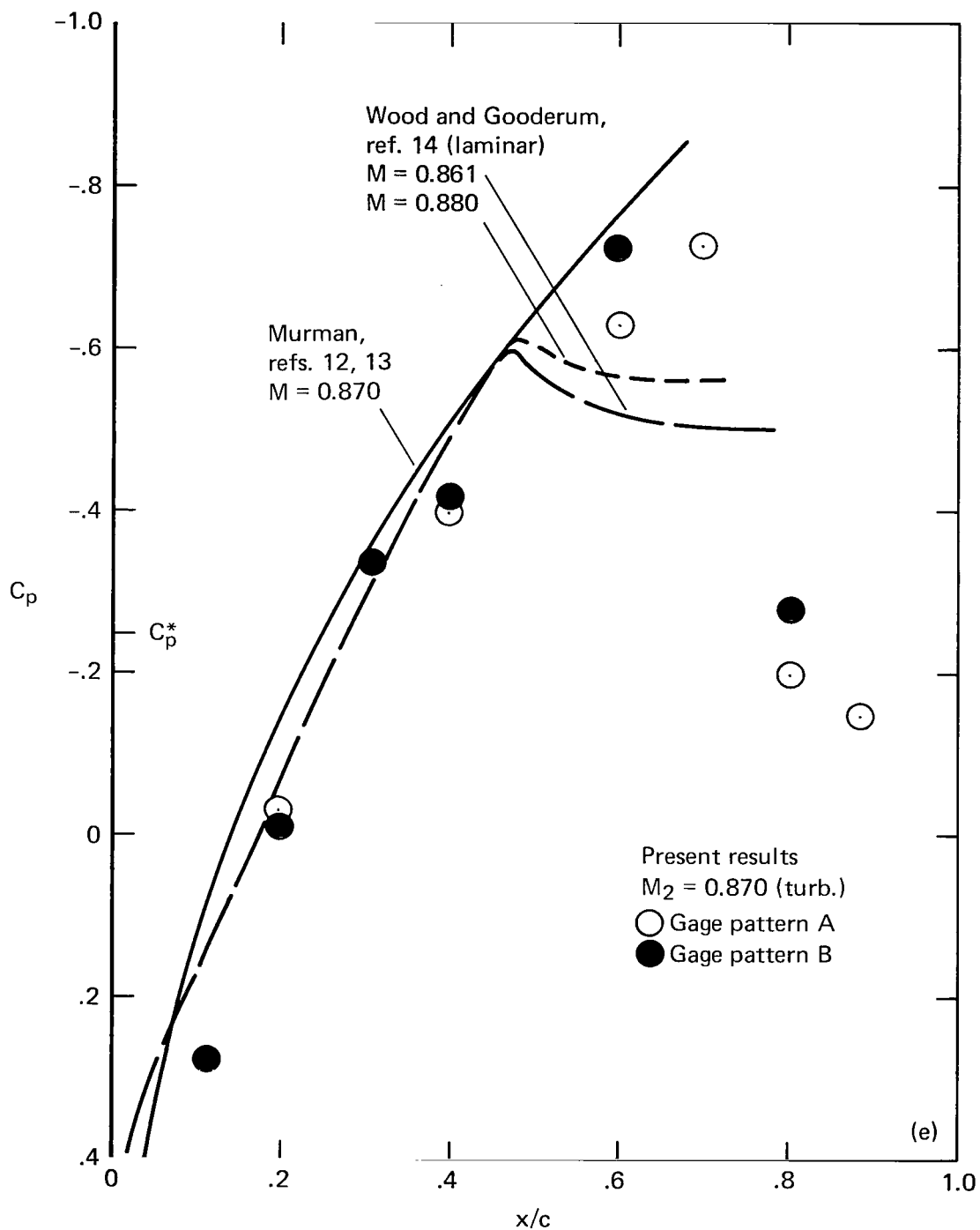
(c) Pressure coefficients vs chord position.
 Present results; $M = 0.830$ wall contour.

Figure 13.- Continued.



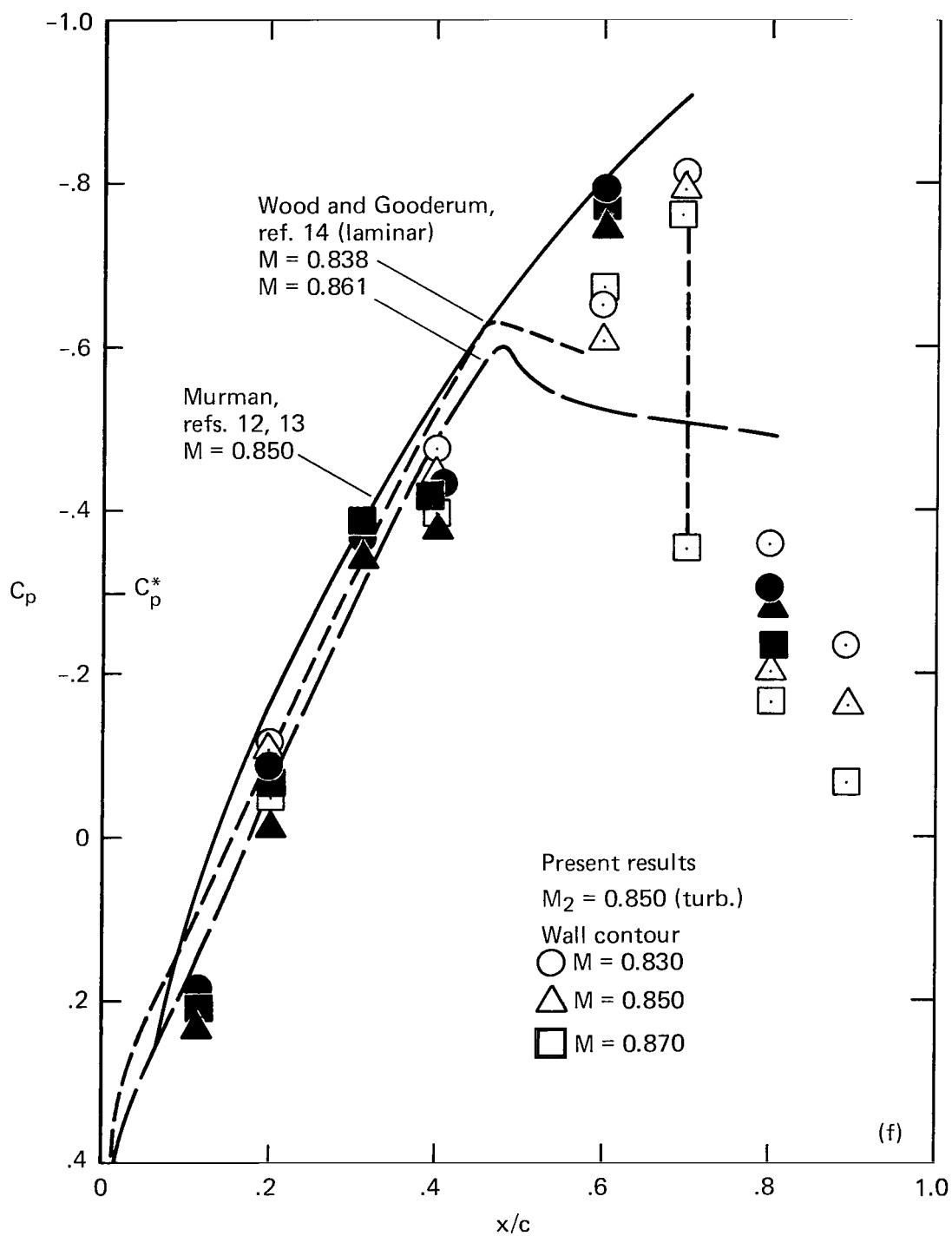
(d) Pressure coefficients vs chord position.
Present results; $M = 0.850$ wall contour.

Figure 13.- Continued.



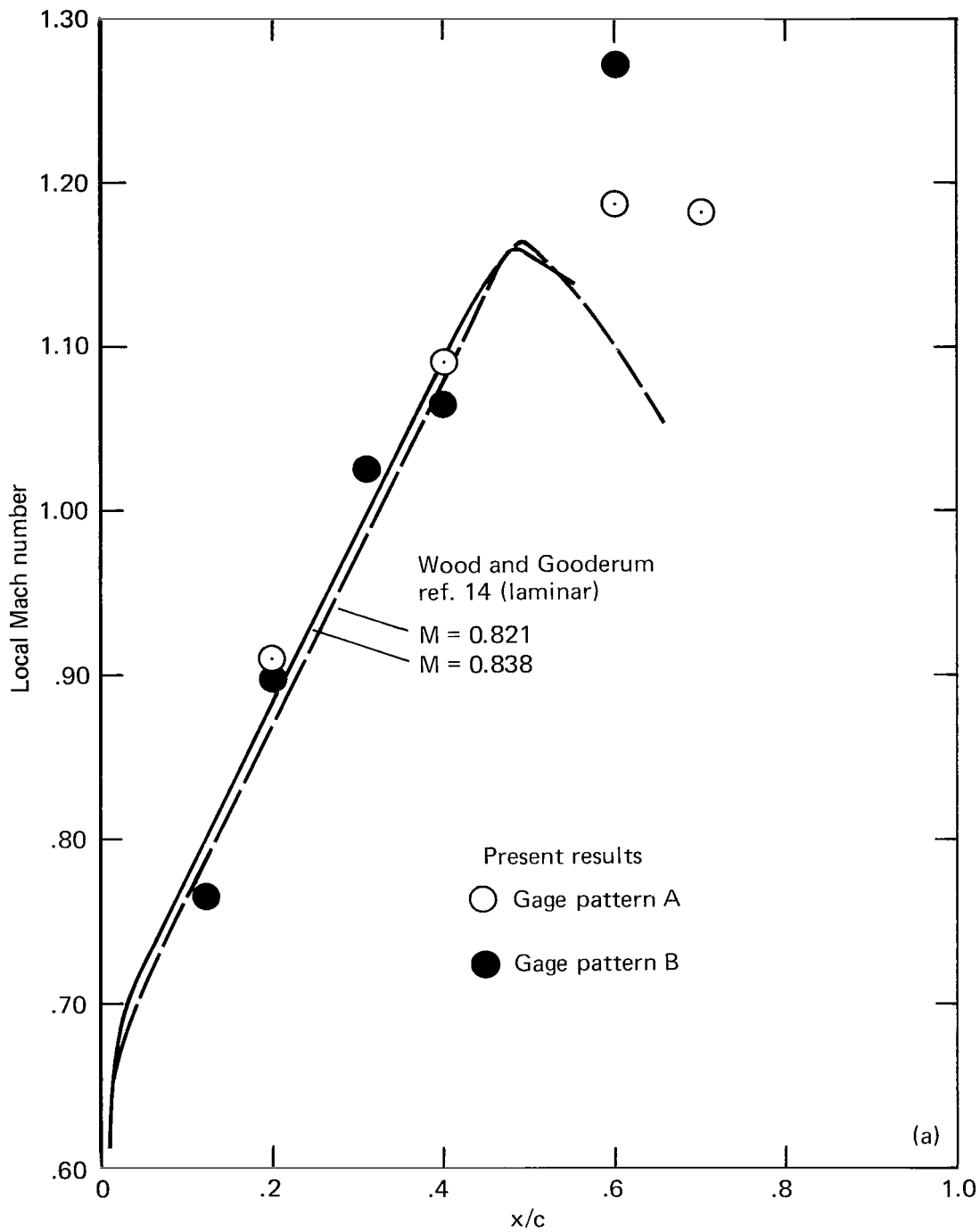
(e) Pressure coefficients vs chord position.
Present results; $M = 0.870$ wall contour.

Figure 13.- Continued.



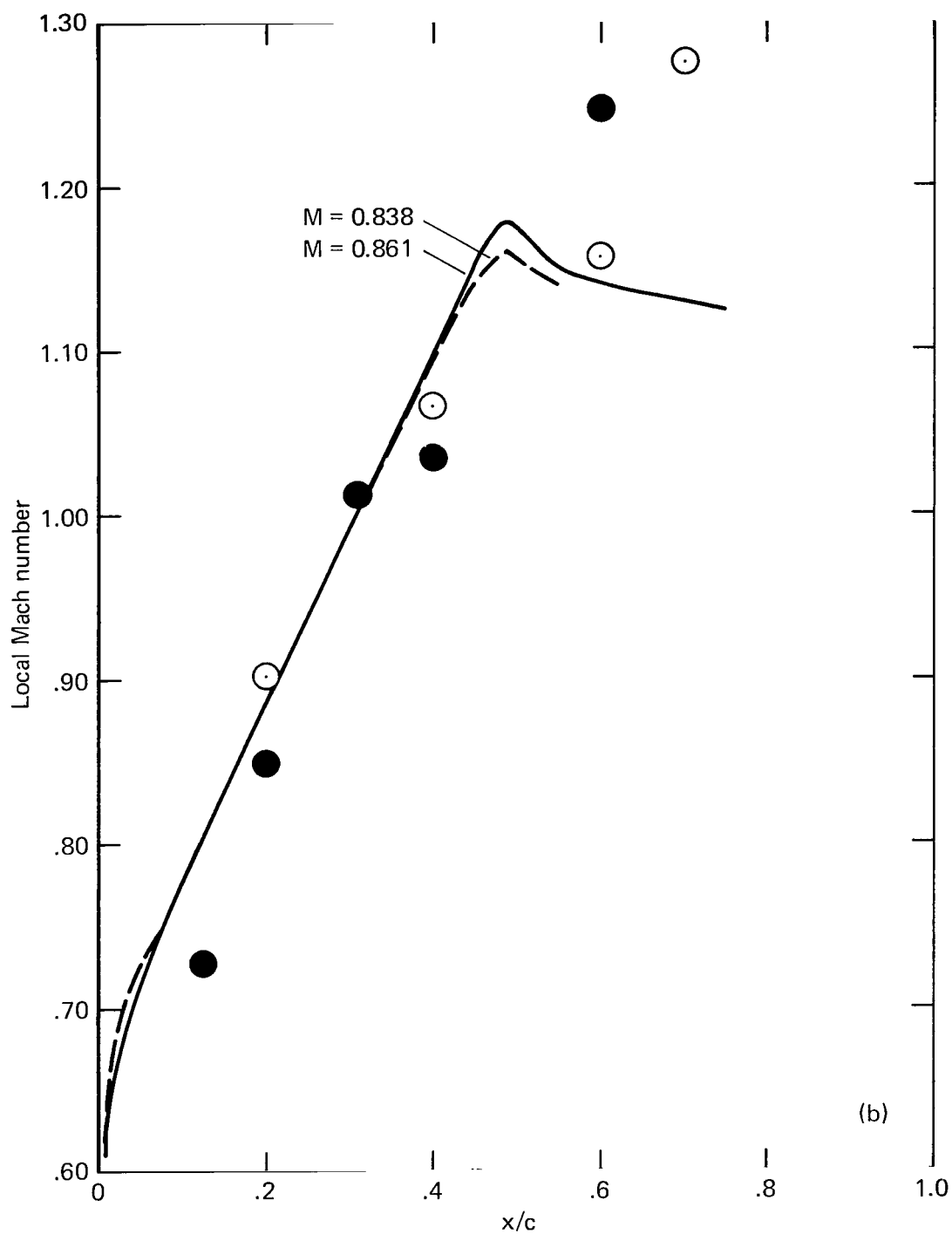
(f) Pressure coefficients vs chord position.

Figure 13.- Concluded.



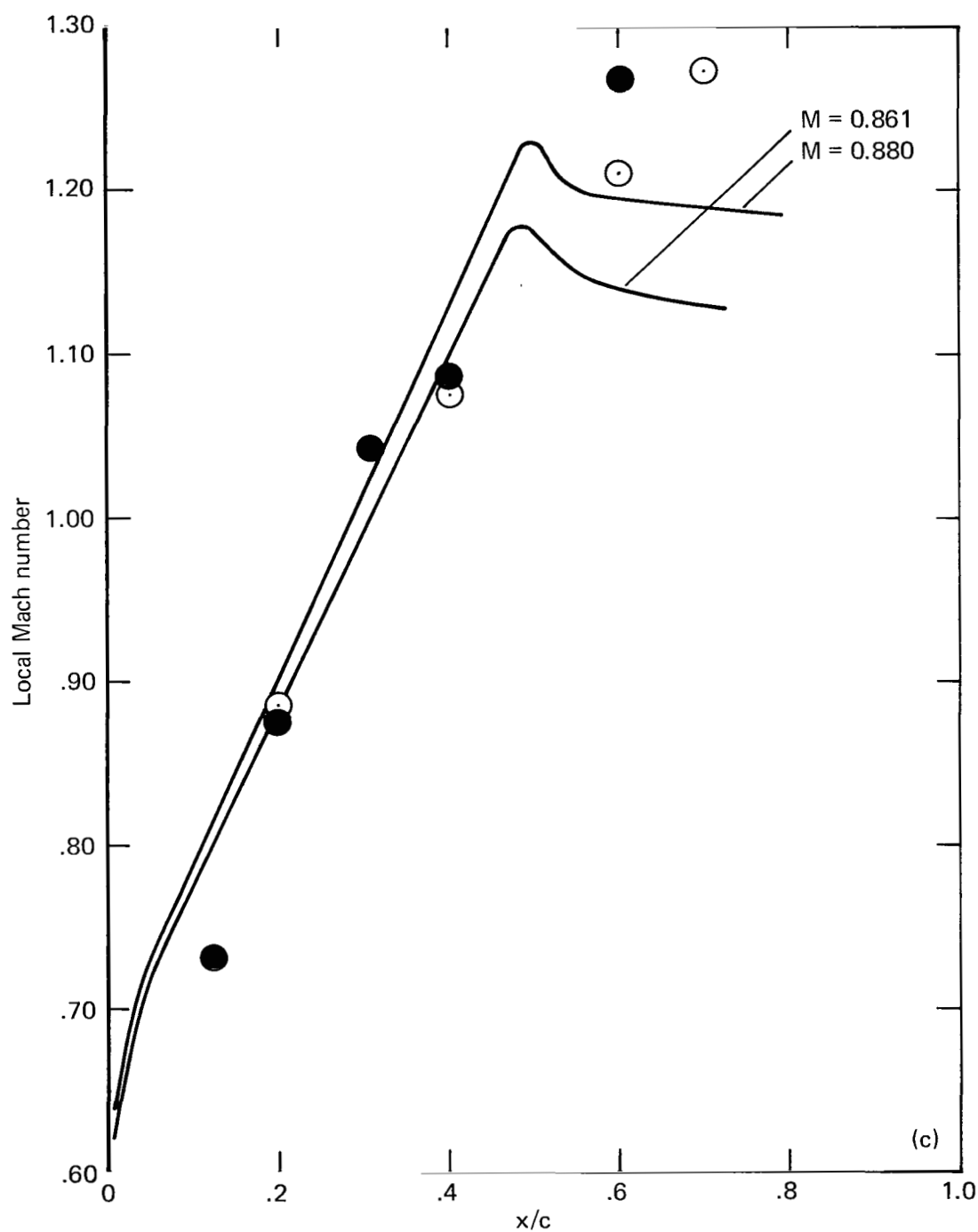
(a) $M_2 = 0.830$. Present results based on C_p values, figure 13(c).

Figure 14.- Comparison of local Mach numbers.



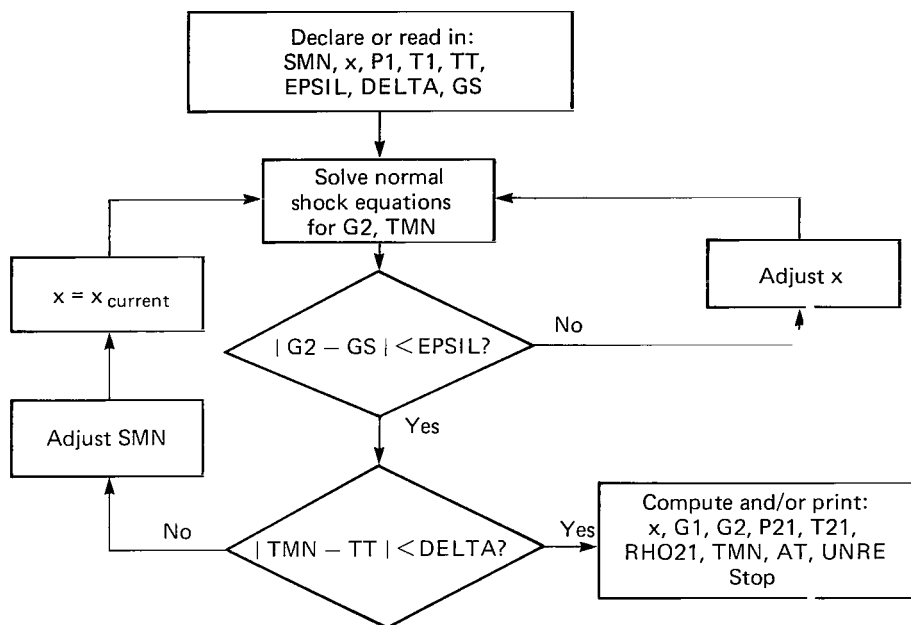
(b) $M_2 = 0.850$. Present results based on C_p values, figure 13(d).

Figure 14.- Continued.



(c) $M_2 = 0.870$. Present results based on C_p values, figure 13(e).

Figure 14.- Concluded.



(a) Flow chart.

<u>Nomenclature Symbol</u>	<u>Program Symbol</u>	<u>Description</u>
M_s	SMN	Shock Mach number
M_2	TMN	Test Mach number
γ_1	G1	Specific heat ratio, region 1
γ_2	G2	Specific heat ratio, region 2
—	GS	Desired value of G2 (= 1.4)
—	EPSIL	Convergence tolerance on G2
—	TT	Desired value of M_2
—	DELTA	Convergence tolerance on M_2
x	x	Mole fraction of argon
P_1	P1	Pressure ahead of shock wave
T_1	T1	Temperature ahead of shock wave
—	AT	$a_1 / (T_1)^{1/2}$
Re/cp_1	UNRE	Reynolds number parameter

(b) Notation for flow chart. (See program listing, table A1, for complete listing of program symbols.)

Figure 15.— Flow chart and notation for computer program for solution of normal shock equations and evaluation of flow parameters for argon-carbon dioxide mixtures.

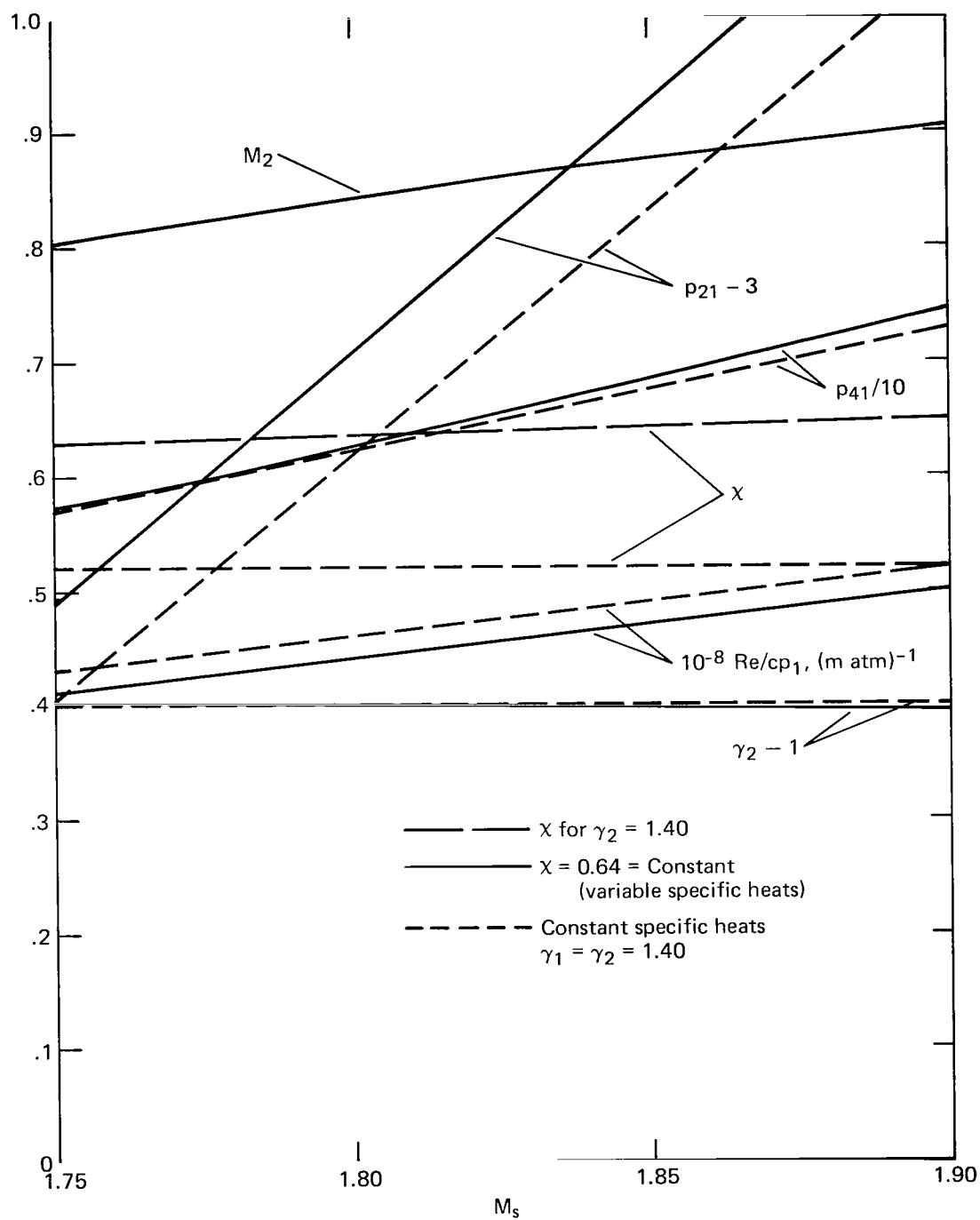


Figure 16.- Results for constant and variable specific heats for argon-carbon dioxide test gas mixtures.

1. Report No. NASA TP-1268		2. Government Accession No.		3. Recipient's Catalog No.	
4. Title and Subtitle APPLICATION OF SHOCK TUBES TO TRANSONIC AIRFOIL TESTING AT HIGH REYNOLDS NUMBERS				5. Report Date November 1978	
				6. Performing Organization Code	
7. Author(s) William J. Cook* and Michael J. Chaney* Leroy L. Presley and Gary T. Chapman				8. Performing Organization Report No. A-6855	
				10. Work Unit No. 505-06-21	
9. Performing Organization Name and Address *Iowa State University, Ames, Iowa 50010, and NASA Ames Research Center Moffett Field, Calif. 94035				11. Contract or Grant No.	
				13. Type of Report and Period Covered Technical Paper	
12. Sponsoring Agency Name and Address National Aeronautics and Space Administration Washington, D.C. 20546				14. Sponsoring Agency Code	
15. Supplementary Notes					
16. Abstract					
<p>The shock tube as a device to fulfill current needs for testing transonic airfoils at high Reynolds numbers is considered. Performance analysis of a gas-driven shock tube shows that transonic airfoil flows with chord Reynolds numbers of the order of 100×10^6 can be produced, with limitations being imposed by the structural integrity of the facility or the model. A study of flow development over a simple circular arc airfoil at zero angle of attack has been carried out in a shock tube at low and intermediate Reynolds numbers to assess the testing technique. Results obtained from Schlieren photography and airfoil pressure measurements show that steady transonic flows similar to those produced for the same airfoil in a wind tunnel can be generated within the available testing time in a shock tube with properly contoured test section walls. The study indicates that the shock tube is an alternative facility for studying high Reynolds number transonic airfoil flows.</p>					
17. Key Words (Suggested by Author(s)) High Reynolds number Airfoil testing Transonic flows Shock tube			18. Distribution Statement		
			Unlimited STAR Category - 02		
19. Security Classif. (of this report) Unclassified		20. Security Classif. (of this page) Unclassified		21. No. of Pages 70	
				22. Price* \$4.50	

National Aeronautics and
Space Administration

Washington, D.C.
20546

Official Business

Penalty for Private Use, \$300

THIRD-CLASS BULK RATE

Postage and Fees Paid
National Aeronautics and
Space Administration
NASA-451



1 1 10,A, 102778 S00903DS
DEPT OF THE AIR FORCE
AF WEAPONS LABORATORY
ATTN: TECHNICAL LIBRARY (SUL)
KIRTLAND AFB NM 87117

NASA

S

POSTMASTER: If Undeliverable (Section 15
Postal Manual) Do Not Retu